Dynamics of Nanoparticles Assembly at the Interface of a Nematic Liquid Crystal Droplet

by

Yining Han

A thesis
presented to the University of Waterloo
in fulfillment of the
thesis requirement for the degree of
Master of Applied Science
in
Chemical Engineering-Nanotechnology

Waterloo, Ontario, Canada, 2015

I hereby declare that I am the sole author of this thesis. This is a true copy of the thesis, including any required final revisions, as accepted by my examiners.

I understand that my thesis may be made electronically available to the public.

Abstract

Up-to-date technological applications of liquid crystal (LC)-based devices have relied on the nematic LC materials in the form of drops or emulsions stabilized by surfactants. Adsorption of nanoparticles at liquid interfaces results in emulsions with exceptional stability. Adsorption of nanoparticles at nematic liquid crystal interfaces provides an alternative promising approach to stabilize nematic emulsions or drops. Improved understanding of the dynamics of the adsorption process of nanoparticles at the nematic LC-water interface is important not only due to its technological significance, but also of interest for the fundamental understanding of non-uniform, ordered fluids. In this work, the dynamic adsorption process of ethyl-cellulose (EC) (with an average radius of 44nm) nanoparticles at the nematic liquid crystal 4-cyano-4'-pentylbiphenyl (5CB) interface is studied by measuring dynamic interfacial tension with the use of a pendant drop tensiometer. Analysis of the dynamic interfacial tension in terms of a model developed by Bizmark et al. (2014) provides information on the adsorption energy $|\Delta E|$ of EC nanoparticles that is compared to the adsorption energy values obtained from two other approaches. We conclude that Bizmark's model for the irreversible adsorption is valid for EC nanoparticle at the isotropic fluid interfaces and also can be applied to study the adsorption of nanoparticles at a nematic liquid crystal interface. Additionally, a model is derived to approximately probe the transient surface (interface) coverage of nanoparticles adsorbed at LC-water interface. Polarized microscopy analysis of 5CB confined between two EC-treated glass substrates confirms that adsorption of EC nanoparticles has no effect on the alignment of 5CB molecules at the interface.

Acknowledgements

I really appreciate the all the kind help and guidance received from my supervisor Marios Ioannidis and professor Nasser M Abukhdeir during the last two years. They help me to build up my confidence to focus on my research, and also help me to go through all the problems with great patience.

I really enjoyed the two years study experience in University of Waterloo. I want to thank all of my dear friends at the department of chemical engineering of University of Waterloo, especially Zhefu Liu and Navid Bizmark, for all their help, support, and valuable hints.

Table of Contents

Chapter 1

Introduction

1.1 Research Motivation

A growing body of technological applications exploiting liquid crystals (LCs) in the form of droplets or emulsions is currently under development. LC-based sensors [1], bacterial biosensors [2], photonic switches [3], microresonators [4,5] and transparent nematic phases [6] are made of composite materials that contain a liquid crystalline phase highly dispersed in an isotropic phase. These applications are enabled by the unique optical properties of LC-in-water emulsions. Unlike conventional isotropic liquids, the orientational order of molecules in LC emulsion droplets usually conforms to three types of orientational textures: bipolar, equatorial, radial and axial [7]. Different orientational textures give rise to different optical responses under crossed polarizers. The type of orienatational ordering of LC molecules is determined by the anchoring strength of LC molecules. A change in the boundary conditions due to the adsorption of surface-active species may trigger an optical response of LCs, which can be directly observed by optical microscopy. This unique optical property of LC droplets has been extensively applied in biological and chemical sensing applications [1,2,8,9].

For technological applications, LC-in-water emulsions are stabilized against droplet coalescence by the addition of surfactants [6,10], nonpolar liquids [11,12], or water-immiscible polymers [12,13]. A number of investigations have focused on the adsorption of surfactants at the LC-water interface [14-18]. Brake *et al*. [14] have confined nematic LC 4-cyano-4'-pentylbiphenyl (5CB) in a copper grid. This approach permits straightforward observation of the orientational change of 5CB molecules at the interface using a polarized optical microscope (POM), which is induced by the reversible adsorption of an amphiphile (sodium dodecyl sulfate) at the LC-water interface. In another work, these authors studied the effect of surfactant molecular structure on the orientation of LC molecules at the interface [17]. Bolaform surfactants, for instance, adopt a looped configuration at the 5CB-water interface resulting in a planar orientation of LCs at the interface. However, long-chain surfactants with a tilted configuration preferentially align the LC molecules perpendicular to the interface (homeotropic alignment). They concluded that the orientation of LC molecules is largely determined by the structure of the hydrophobic moiety of the adsorbed surfactants, whereas the hydrophilic head does not influence orientational order. Considering a reverse approach, a recent computational work [18] considered 5CB as a substrate to study the interfacial arrangement of surfactants at the LC-water interface. Ordered phases at the interface are expected to form by surfactants, which might provide a template for hierarchical self-assembly of more complex-structured materials.

Like surfactants, colloidal nanoparticles can also be used for adsorption at liquid-liquid interfaces for stabilizing emulsions. The adsorption strength of nanoparticles can be much stronger than that of surfactants, resulting in water-in-oil or oil-in-water emulsions of exceptional stability [19,20]. Nanoparticle-stabilized emulsions have been widely applied in a various fields including but not limited to food science, biomedicine, sensing, and catalysis [20-26]. Their application to emulsions involving LCs, however, is only now beginning to be explored [22,23]. A recent computational work by Rahimi *et al*. [22] predict that nanoparticles adsorb at the interface of nematic LCs with a hexagonal ordering. Experimental work provides further insight into the origin of such an

arrangement [23]. For colloidal particles already attached to the interface, the formation of hexagonal arrays in the vicinity of surface defects in the bipolar configuration is explained in terms of three key interactions: (i) splay attraction, (ii) inter-colloid quadrupole-quadrupole elastic interaction, and (iii) interparticle electrostatic repulsion between colloids attached to the interface [23]. The extent to which these interactions may influence the dynamics of self-assembly of nanoparticles at the LC-water interface is presently unknown.

The magnitude of the reduction in free energy, $|\Delta E|$, associated with the transfer of a spherical particle from the bulk phase to the fluid-fluid interface is given by the following equation [19]:

$$|\Delta E| = \gamma_0 \pi r^2 \left(1 - |\cos\theta|\right)^2 \tag{1}$$

where r is the radius of the particle, γ_0 is the interfacial tension of the pristine fluid-fluid interface and θ is the contact angle of a particle at the fluid interface measured through the aqueous phase. An alternative approach to Eqn. (1) for estimating the adsorption energy is suggested on the basis of simple thermodynamic arguments [25]:

$$|\Delta E| = \frac{\gamma_0 - \gamma_\infty}{\Theta_\infty} \pi r^2 \tag{2}$$

In Eqn. (2), γ_∞ and Θ_∞ are the interfacial tension and fractional coverage of the interface at steady state, respectively. In the absence of other information, a value of $\Theta_\infty = 0.91$, which corresponds to the hexagonal close packing of particles at the interface, has been assumed in order to estimate $|\Delta E|$ [25]. Recently, Bizmark et al. [26] have developed a mechanistic model to interpret two asymptotic stages (early: $t \to 0$ and late: $t \to \infty$) of the adsorption process:

$$t \to \infty: \quad \gamma = \gamma_0 - 2N_A |\Delta E| C_0 \sqrt{\frac{Dt}{\pi}} \tag{3}$$

$$t \to \infty: \quad \gamma = \gamma_\infty + \frac{K_l |\Delta E|}{\left(\pi r^2\right)^2 N_A C_0} \sqrt{\frac{1}{Dt}} \tag{4}$$

where N_A is Avogadro's number, C_0 is the molar bulk concentration, and D is the nanoparticle diffusion coefficient, which can be estimated from the Stokes-Einstein equation ($D = k_B T / 6\pi\mu r$) [27], given the solvent viscosity (μ) and the temperature (T). In Eqn. (4), K_l is a parameter defined in terms of the maximum coverage of the interface (Θ_{max}) and the adsorption rate constant (k_a) as follows:

$$K_l = \Theta_{max}\left(\Theta_{max} / 4.64 k_a\right)^{1/2} \tag{5}$$

Employing the asymptotic model at early stages of adsorption reported by Bizmark et al. [26] (Eqn. (3)), one can compute the adsorption energy exclusively from dynamic interfacial tension data, without reference to contact angle (viz. Eq. (1)) or steady-state surface coverage (viz. Eq. (2)).

1.2 Objectives of This Work

The objectives of this research are to:

(1) measure the dynamic interfacial tension of nematic liquid crystal 5CB with adsorption of ethyl cellulose nanoparticles by pendant drop tensiometer;

(2) analyze the dynamic interfacial tension data with Bizmark's model, revealing information of early time interfacial tension γ_0, late time interfacial tension γ_∞ and adsorption energy $|\Delta E|$;

(3) apply the results obtained from Bizmark's model to other two models, and compare the adsorption energy $|\Delta E|$ obtained via those different approaches;

(4) use polarized microscope to investigate the effect of EC nanoparticles on the orientational ordering of 5CB molecules at the water-LC interface.

In this work, pendant drop tensiometry [28] is used to probe the dynamic adsorption of negatively charged ethyl cellulose (EC) nanoparticles at 5CB-water interface. Dynamic interfacial tension data, complemented by measurements of the 5CB-water contact angle on EC-coated substrates are analyzed to determine the adsorption

energy, steady state interfacial tension, and ultimate surface coverage. It is found that the orientational order of 5CB at the LC-water interface remains planar despite the fact that the interface becomes densely covered by EC nanoparticles, with Θ_{max} approaching the hexagonal close-packing limit. These results have significant implications for the quantitative description of nanoparticle self-assembly at LC interfaces.

Chapter 2

Background

2.1 Overview

Research on liquid crystal phases has been continuously conducted over the past 80 years. Liquid crystals are a state of matter like solid, liquid and gases. Scientifically, the documentation and understanding of the physical phenomena found in liquid crystal phases have attracted significant interest. Technologically, liquid crystals have gradually become a part of our daily lives, since they are widely used for displays, such as televisions and computers. As a consequence, liquid crystals play a significant role scientifically and technologically. It is both necessary and informative to have a basic

understanding of how this phase of matter behaves and can be utilized for technological applications.

The person generally given credit for discovering liquid crystals is an Austrian botanist, Friedrich Reinitzer. Reinitzer's primary interest was to examine the physicochemical properties of various derivatives of cholesterol in plants. In 1888, Reinitzer found that cholesteryl benzoate (structure as shown in Figure 2.1) possessed two melting points; 145.5 °C (293.9 °F) at which it melts into a cloudy liquid, and 178.5 °C (353.3 °F) where it re-melts from a cloudy liquid to clear one. The phenomenon is reversible. And he also observed some unusual optical behavior of this liquid crystal upon cooling; first a pale blue color appeared as the liquid crystal turned cloudy and then a bright blue-violet color appeared as the liquid crystal crystallized. Reinitzer sent samples of this substance to Otto Lehmann to examine. Lehmann conducted his own experiments and confirmed Reinitzer's observation on his heating stage microscope with crossed polarizers. Based on his observations, he saw some connections between this sample and crystalline matter. He gradually became more convinced that the cloudy fluid had crystalline properties. This combination of features, namely that it flowed like liquid but affected the polarized light in a manner typical of solid crystalline, finally led Lehmann to name these substances " liquid crystals ".

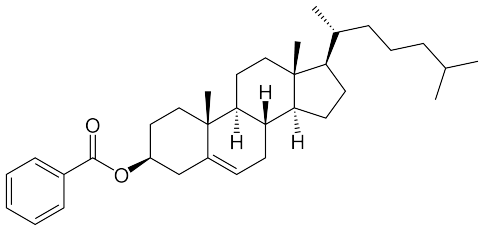

Figure 2.1 Structure of cholesteryl benzoate in ref. [1].

From the 1930s to 1940s, research on liquid crystals, mainly focused on their elastic properties, crystalline structure and the effects of the electric and magnetic fields. Later, research on liquid crystals stagnated because they were considered not to have any useful application. However, shortly after 1960, with realizations of the scientific significance and potential applications of liquid crystal, work on liquid crystal increased

again. Liquid crystals are widely used in liquid crystal displays, liquid crystal thermometers and temperature-sensing films, high-strength liquid crystal polymers, and surfactants for the oil recovery industry, etc. A growing body of technological applications of liquid crystals (LCs) have recently been demonstrated, such as bacterial biosensors, photonics switches, microresonators and transparent nematic phase, which has triggered a great interest in research on LC-in-water and water-in-LC emulsions. Another example of LC are polymer-dispersed liquid crystals (PDLC), which are LC composites used as electrically-switchable private windows. All those fascinating applications have generally relied on surface-dominated composite materials that contain a liquid crystal phase in close contact with an isotropic phase. In order to prepare those composite materials, it is important to understand the interfaces between the liquid crystalline phase and the isotropic phase to determine the degree of phase segregation.

2.2 Introduction to Liquid Crystal

Materials in nature can be divided into different phases or states of matter. The three most common states of matter are solids, liquids and gases. The difference between crystals and liquids, the two most common condensed matter phases, is that the molecules in a crystal are ordered in a lattice and oriented in a specific direction by strong intermolecular forces, whereas in a liquid they are not. In a liquid, the molecules undergo random motion molecular axes varying as shown in Figure 2.2. Although it seems like those three categories of states of matter are very well defined, the borders between these different states are actually not that clear. Interestingly enough, besides these main phases of matter, there also exist in nature many intermediate states or mesophases, whose order is more than what is observed in liquids but less than what is observed in crystals. Those phases are called liquid crystalline, since they share properties associated with both liquid and crystals. For instance, a liquid crystal material may diffuse like a liquid, but as it maintains some degree of orientational order.

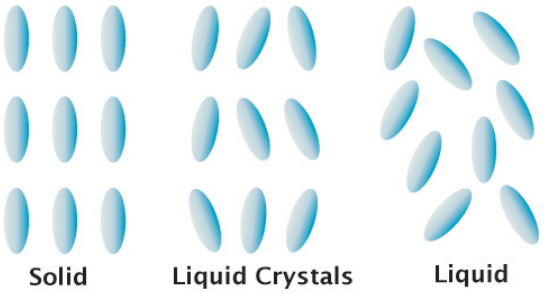

Figure 2.2 Schematic illustration of Solid, liquid crystal and liquid molecules orientation in ref. [60].

The distinguishing characteristic of the liquid crystalline phases, specifically nematic LC phase, is that the molecular axis in LCs tends to point along a preferred direction, called the director. The amount of order in a liquid crystal is quite small compared to a solid crystal. To quantify the amount of orientation order in a liquid crystal phase, an average orientational order parameter of liquid crystal is defined as follows:

$$S=\left\langle \frac{3}{2}\cos^2\theta-\frac{1}{2}\right\rangle \tag{6}$$

where θ is the angle between the director and the long axis of each molecule as shown in Figure 2.3. The brackets denote an average over all of the molecules in the sample.

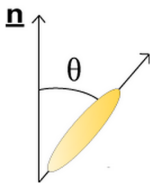

Figure 2.3 Schematic showing the angle θ between the director and the long axis of each Molecule.

When $S=1$ the liquid crystal has complete orientational order; when $S=0$, the liquid crystal has no orientational order and it becomes an isotropic liquid like water or oil. The characteristic orientational order of the liquid crystal state is between that of the traditional solid and liquid phases is the origin of the term mesogenic state. In an isotropic liquid, the average of the cosine terms is zero, and therefore the order parameter is equal to zero. For a perfect crystal, the order parameter evaluates to one. Typical values

for the order parameter of a liquid crystal range between 0.3 and 0.9 [66].

2.3 Types of Liquid Crystals

There are many types of liquid crystal phases. Generally, liquid crystal phases can be classified into three categories: nematic, cholesteric and smectic, depending on the amount of order of the liquid crystal. What they all have in common is that all those liquid crystals are anisotropic.

2.3.1 Nematic Liquid Crystal.

The simplest type of liquid crystal is nematic liquid crystal. In the nematic phase, the rod-like liquid crystal molecules have no positional order but tend to align themselves in the same direction (along the director) as shown in Figure 2.4. The nematic liquid crystal is free to flow, but still maintains long-range orientational order. Under a polarized microscope, nematic liquid crystals often shows many dark lines, and those lines are called defects or disclinations. The preferred alignment of liquid crystal along these defects is undefined. Nematic liquid crystals have been widely applied in a variety of technological applications. In fact, most liquid crystal devices make use of nematic liquid crystals.

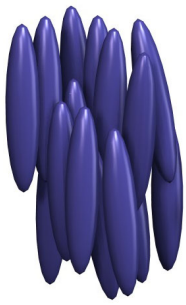

Figure 2.4 Schematic showing molecule alignment in the nematic liquid crystal in ref. [59].

2.3.2 Cholesteric Liquid Crystal

A cholesteric LC phase has a layer structure as shown in Figure 2.5. In each layer, the cholesteric liquid crystal is very similar to the nematic liquid crystal. The molecules in a cholesteric liquid crystal phase can only be chiral. In cholesteric phase, chiral molecules cause a twist in the nematic structure. At the same time, molecules in each layer are tilted by a finite angle. The unique property of cholesteric liquid crystals is that they reflect circularly polarized light when it is incident along the helical axis and elliptically polarized if the incident light comes in oblique way.

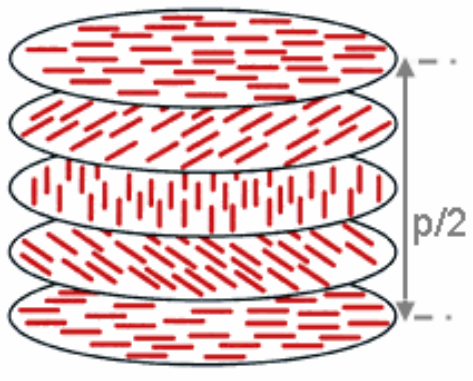

Figure 2.5. Schematic of cholesteric liquid crystal in ref. [59].

2.3.3 Smectic Liquid Crystal

Another common LC phases are the smectic phases. In addition to the orientational order of nematic liquid crystals, smectic LCs have positional order where they tend to arrange in layers as shown in Figure 2.6. Smectic LCs include smectic A phases and smectic C phases. If the molecules are oriented perpendicular to the layer, it is a smectic A phase. In the smectic C phase, liquid crystal molecules are tilted inside the layers. In these two smectic phases, there is no positional order within the layers.

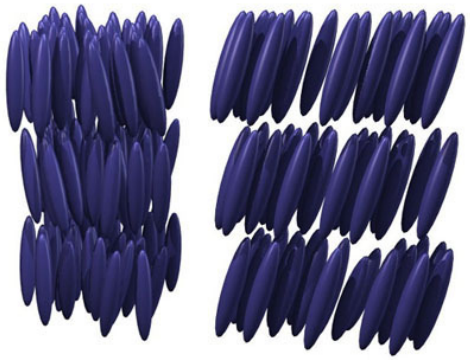

Figure 2.6 Schematic of alignment in the smectic phases. The smectic A phase (left) has molecules organized into layers. In the smectic C phase (right), the molecules are tilted inside the layers in ref. [59].

2.4 Anisotropy of Liquid Crystals

The characteristic property of liquid crystals that distinguishes them from other phases is their anisotropy, which means the physical properties of liquid crystal are not equivalent in different directions. For example, viscosity, refractive index, dielectric permittivity, magnetic susceptibility, and conductivity all have different values parallel to the director and perpendicular to it. A uniaxial liquid crystal possesses two principal refractive indices: one is called the ordinary refractive index n_o, and the other is called the extraordinary refractive index n_e as shown in Figure 2.7. The ordinary refractive index, n_o, is measured when the electric vector of the light waves vibrates perpendicular to the optical axis. The extraordinary refractive index, n_e, is measured when the electric vector of light waves vibrates along the optical axis.

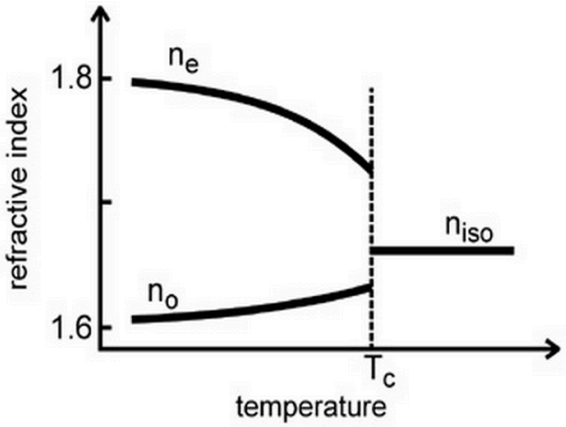

Figure 2.7 Temperature dependence of refractive index: T_c –nematic-isotropic transition temperature; n_{iso} -refractive index of isotropic liquid in ref. [67].

Most nematic liquid crystal phases are optically positive, meaning that the index of refraction parallel to the optical axis, $n_{\|}$, is larger than the index that is perpendicular to the optic axis, $n_{\perp}$ (that is, $\Delta n = n_{\|} - n_{\perp} > 0$). For an optically negative liquid crystal, the reverse is true. Figure 2.8 illustrates uniaxial optically positive and negative liquid crystals [29].

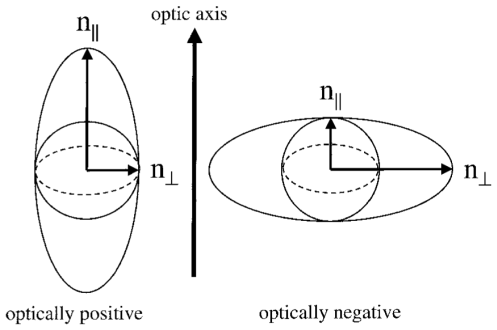

Figure 2.8 Illustration of a uniaxial, optically positive (left) and optically negative (right) liquid crystal molecule in ref. [29].

The optical anisotropy of LC phases causes the unpolarized light incident upon a LC to split into ordinary and extraordinary waves, propagating at a different velocity in the liquid crystal materials as shown in Figure 2.9. The ordinary ray follows Snell's law

of refraction, while the extraordinary ray does not [29,30]. Therefore, liquid crystals are birefringent (double refraction). The light emitting from LC phases will have a phase difference, which is given by [29]:

$$\delta = \frac{2\pi}{\lambda}\left(n_e - n_o\right)d \tag{7}$$

where λ is the vacuum wavelength and d is the distance traveled in the medium or material thickness. The indices of refraction n_o and n_e are related to the principal indices of refraction $n_{\parallel}$ and $n_{\perp}$ according to the following equation [29]:

$$n_e = n_{\perp} \tag{8}$$

and

$$n_e = \frac{n_{\parallel} n_{\perp}}{\sqrt{n_{\parallel}^2 \cos^2\phi + n_{\perp}^2 \sin^2\phi}} \tag{9}$$

where ϕ is the angle between the optical axis and the direction of the light propagation.

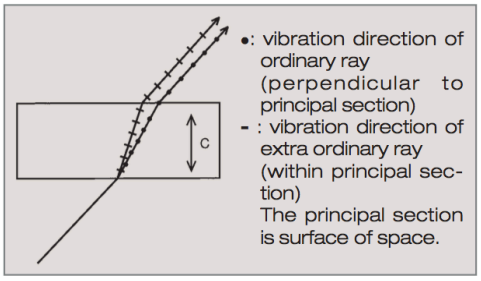

Figure 2.9 Vibration direction of ordinary rays and extraordinary rays of anisoptically uniaxial liquid crystal in ref. [30].

2.5 Nematic Liquid Crystal Textures

For research on the textures of LC phases, they are conventionally enclosed into a transparent planar cell, and then the optical cell is observed under polarized microscope with crossed polarizers. When the molecular director aligns parallel to the substrate surface, a "Schlieren" texture organized around point disclinations is observed under

polarized microscope with crossed polarizers as shown in Figure 2.10 (a). In a homeotropically aligned liquid crystal texture, where the liquid crystal molecular director is perpendicular to the substrate surface, no birefringence (totally dark) is observed, as shown in Figure 2.10 (b).

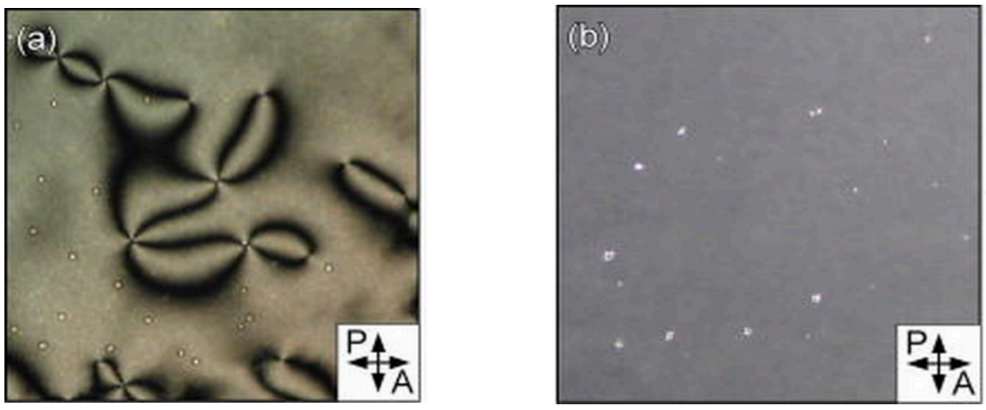

Figure 2.10 Photomicrographs of the Nematic phase (E31 at room temperature). (a) Schlieren texture in a 20-micron planar cell. Plus and minus 1 point disclinations and plus and minus half disclinations are apparent. (b) Homeotropically aligned texture in a 100-micron cell of substrates coated with OTE monolayer in ref. [61].

Schlieren textures are characterized by sets of curved dark brushes, as shown in Figure 2.10 (a). These dark brushes correspond to the extinction position of nematic director fields, when they are parallel to the direction of either the polarizer or the analyzer. All the dark brushes come together at singular points that are topological defects.

2.6 Introduction to Nematic Liquid Crystal Droplet Configurations

Molecules in LC droplets usually adopt four types of orientational ordering: bipolar, axial, radial and equatorial configurations [68,69] as shown in Figure 2.11. The anchoring model in radial and axial configuration is perpendicular, which means the LC molecules prefer to orient themselves normal to the boundary surface or interface, while the anchoring model in bipolar and equatorial configuration is parallel to the surface or

interface. The type of oritentational ordering of LCs is largely determined by boundary condition and anchoring strength of LC molecules. For example, if the LC molecules adopt a strong hometropic anchoring, that is, the director of the LC molecules is fixed vertically to the droplet interface, the droplet configuration compatible with the boundary condition is the radial with a single point defect can be observed at the center of the droplet under crossed polarizers. The axial configuration of the LC droplets also occurs when the LC molecules are oriented perpendicular to the droplet interface, but only when the surface anchoring strength is weak, and no defects can be observed under crossed polarizers [69]. For LC molecules in bipolar configuration, an optical texture with two points defects in opposite directions can be viewed under crossed polarizers. This characteristic optical property of LC emulsions has been widely used in biological and chemical sensing applications [1-6].

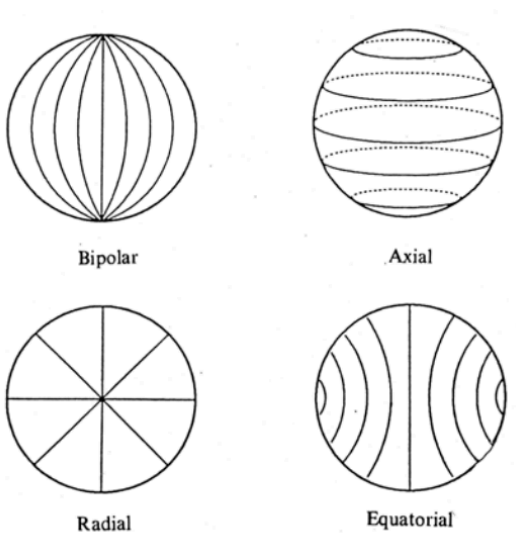

Figure 2.11. Four typical director configurations of nematic` droplets in ref. [68].

2.7 Ethyl Cellulose

Liquid crystals have been generally employed in technological applications in the form of emulsions or droplets, which usually require the addition of surfactants to inhibit drop coalescence. Similar to surfactants, solid colloidal particles can also adsorb at gas-

liquid and liquid-liquid interfaces, and used to stabilize so-called "Pickering" emulsions. In this work, the solid particle used to adsorb at the water-LC interface is ethyl cellulose, which is derived from cellulose. Its basic structure is shown in Figure 2.12. EC nanoparticles are hydrophobic and charge-stabilized at a neutral pH [26].

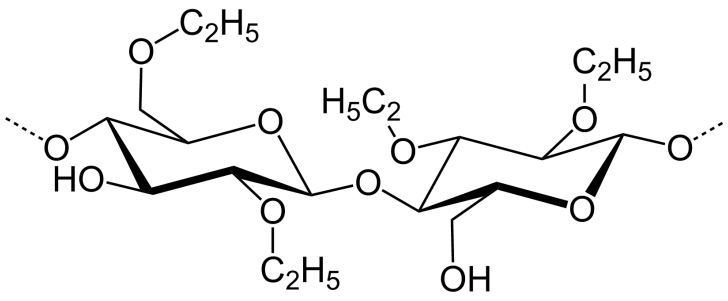

Figure 2.12. The basic structure of ethyl cellulose in ref. [62].

2.8 Adsorption Energy Models

The dynamic interfacial tension data for nanoparticle colloidal solution have been studied in term of the classical model of Ward and Tordai [32]:

$$t \to 0: \quad \gamma = \gamma_0 - 2RTC_0\sqrt{\frac{Dt}{\pi}} \tag{10}$$

$$t \to \infty: \quad \gamma = \gamma_\infty + \frac{RT\Gamma_\infty^2}{C_0}\sqrt{\frac{\pi}{4Dt}} \tag{11}$$

Here, R is the gas constant, T is the temperature, C_0 is the molar bulk concentration of colloidal particles, Γ_∞ is the molar surface concentration at steady state, and D is the nanoparticles diffusion coefficient. However this model is not capable of interpreting dynamic interfacial tension data when the adsorption energy of particles exceeds the mean energy of thermal fluctuations ($|\Delta E| \gg k_B T$), which indicates that the adsorption process is irreversible. Bizmark et al. validated an alternative model to study the irreversible adsorption as following [26]:

$$t \to 0: \quad \gamma = \gamma_0 - 2N_A \left|\Delta E\right| C_0 \sqrt{\frac{Dt}{\pi}} \tag{3}$$

$$t \to \infty: \quad \gamma = \gamma_\infty + \frac{K_l \left|\Delta E\right|}{\left(\pi r^2\right)^2 N_A C_0} \sqrt{\frac{1}{Dt}} \tag{4}$$

Equation (3) is applied to analysis the early stages ($t \to 0$) of the adsorption of EC nanoparticles by plotting dynamic interfacial tension γ against $\sqrt{t}$. Equation (4) is used to study the late stages ($t \to \infty$) of the adsorption of EC nanoparticles by plotting dynamic interfacial tension γ against $1/\sqrt{t}$.

Another two approaches from previous studies can be used to estimate the adsorption energy of solid particles adsorbed at gas-liquid and liquid-liquid interfaces as following:

$$\left|\Delta E\right| = \gamma_0 \pi r^2 \left(1 - \left|\cos\theta\right|\right)^2 \tag{1}$$

$$\left|\Delta E\right| = \frac{\gamma_0 - \gamma_\infty}{\Theta_\infty} \pi r^2 \tag{2}$$

Equation (1) relates the reduction of surface energy ($\left|\Delta E\right|$) associated with the radius r of adsorbed spherical particles and contact angle θ [19]. Equation (2) relates the reduction of surface energy ($\left|\Delta E\right|$) associated with fractional surface coverage Θ [25].

Chapter 3

Literature Review

3.1 Current Applications of Liquid Crystal Emulsions and Droplets

Liquid crystals emulsion-based materials are emerging as promising candidates for a group of sensing and interfacial applications because of their large surface area compared to planar interfaces and unique optical properties [7,33]. Technological applications of liquid crystals have generally relied on control of their molecular orientation at a surface or an interface. A growing body of technological applications of liquid crystals (LCs) droplets or emulsions has recently been demonstrated, such as bacterial biosensors [2], photonic switches [3], microresonators [4,5] and transparent nematic phases [6]. These fascinating applications have triggered a great interest in studying water-in-LCs, LCs-in-water emulsions. Sivakumar et al. [8] presented a novel and versatile method based on monodisperse liquid crystal emulsion droplets, which can

be employed to detect and distinguish biological bacteria and viruses, as demonstrated in Figure 3.1:

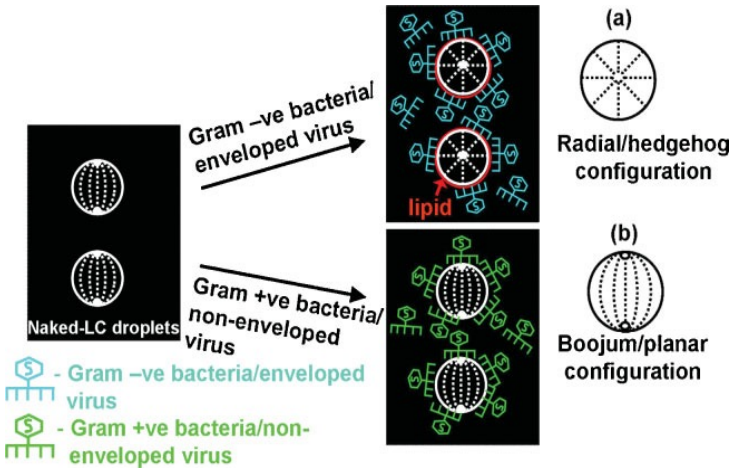

Figure 3.1 Schematic illustration of the interaction of bacteria or viruses with naked LC emulsions. The cartoons depict the **a)** radial and **b)** bipolar configurations of LC droplets in ref. [8].

Three different bacteria — Escherichia coli [8] (E. coli, gram -ve, with outer membrane), bacillus subtilis (B. subtilis, Gram +ve, without outer membrane), and micrococcus luteus (M. luteus, Gram +ve) — and two different viruses — M13 helper phage (non-enveloped) and A/ NWS/Tokyo/67 (enveloped) were chosen to be in contact with monodisperse nematic LC droplets (4-cyano-4'-pentylbiphenyl, 5CB). These bacteria and viruses possess distinct structural differences. E. coli and B. subtilis are rod-shaped, M. luteus is a spherial, M13 helper phage exhibits an icosahedron structure, while A/NWS/Tokyo/67 is bullet-shaped. They found that configuration transitions of the 5CB LC droplets from bipolar to radial occurred in contact with gram -ve bacteria (E. coli) and lipid-enveloped viruses (A/NWS/Tokyo/67), due to the transfer of lipid from their surfaces to that of the LC droplets. This method should be very useful for screening a very large number of biological samples based on their structural features.

Fernández-Nieves et al. [3] reported a method for the formation of photonic devices possessing electro-optic properties which enable them to change from an opaque, and Bragg diffracting state to a transparent one continuously at a moderate electric (E) fields.

This electro-optic property is based on dispersing uniform micrometer sized droplets of nematic LC 5CB in an aqueous polymer solution, stabilized with 1wt% polyvinyl alcohol (PVA), which permits a strong planar anchoring of the LC at the surface. The uniform LC droplets are randomly disordered in the beginning as shown in Figure 3.2(b), but eventually self-assemble into an ordered colloidal structure through sedimentation into a hexagonal layer as shown in Figure 3.2(c). The continuous water phase is evaporated and liquid crystal drop is encapsulated by a PVA wall as shown in Figure 3.2(d). This fabrication is different from conventional polymerization induced phase separation employed in fabrication of polymer-dispersed liquid crystals (PDLCs). When no electric field is applied, the polar axis of every drop is randomly oriented and the resulting optical appearance is opaque as shown in Figure 3.2(b); Applying an electrical field normal to the hexagonally close packed planes, results in a Bragg diffraction pattern as shown in Figure 3.2(c). When the E field is large enough, the optical appearance becomes transparent as shown in Figure 3.2(d). The use of highly monodisperse LC emulsions drops facilitates self-assembly of ordered arrays, makes Bragg diffraction easily achievable.

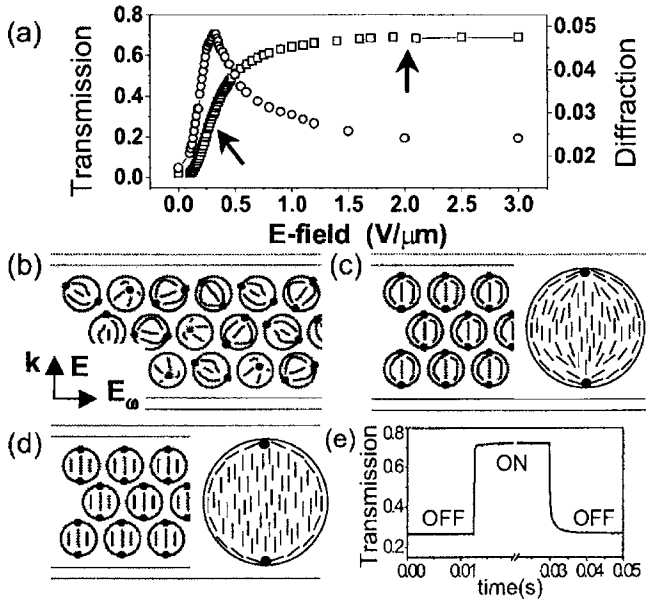

Figure 3.2 Schematics of the switching mechanism: **(b)** E=0, the polar axis of every drop is randomly oriented and the structure is opaque; **(c)** E =0.32 V/ μm, the polar axis of every drop is aligned with E and the system Bragg diffracts; **(d)** E >2.0V/μm, index matching between the drops and the matrix renders the structure transparent. In (b) and (c) a cross section of the

bipolar drop illustrates the microscopic states in ref. [3].

Liquid-crystal microresonators consist of spherical nematic LC E12 (a commercial mixture of cyanobiphenyl (NLCs) microdroplets suspended in a transparent rubber polymer polydimethyl-siloxane (PDMS) matrix [5], as shown in Figure 3.3. To work as an optical microresonator, the liquid-crystal molecules are forced to orient themselves perpendicular to the LC-PDMS interface without an electric field. The liquid crystal orientation is radial with a point defect at the center. The anchoring direction of LC is indicated by solid dark line. When light travels along the meridian of the sphere, the liquid crystal orientation aligns with the optical vector (white arrows). Under this condition, it is easier to meet the condition of the total internal reflection. When a strong electrical field is applied, the liquid crystal orientation does not match that of the optical electric vector, and so total internal reflection is hard to achieve, resulting in a shift towards shorter wavelengths.

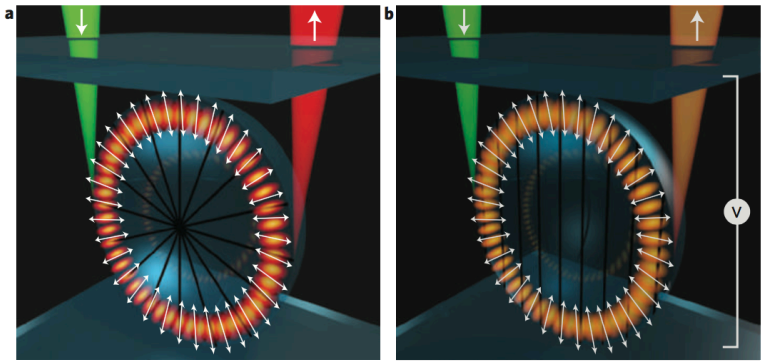

Figure 3.3 Cross-sectional view of the whisphering-gallery-mode (WGM) microrensonator formed from a nematic liquid crystal droplet. **(a)** The initial state without an electric field and **(b)** shift in wavelengths resulting from an applied electric field in ref. [5].

All these fascinating applications of LCs-based devices have generally relied on a surface-dominated composite material, in which an anisotropic liquid crystalline phase is in intimate contact with an isotropic phase. These applications are enabled by the unique optical properties of LC-in-water emulsions. The ordering of LCs is remarkably sensitive

to interfacial events on the scale of molecular level that occur at the LC interface. Any distinct interfacial event may trigger a change in orientation of LC molecules at the surface or interface. This change in orientation is able to propagate to the LC molecules in the bulk (up to 100μm) [33,34] owing to its anisotropic nature. As a result, any ordering transformation of molecules at the interface will result in changes in the optical appearance of LCs, which can be directly examined by optical microscopy as we mentioned before. Technological application of LC molecules droplets has relied on two types of orientational ordering: bipolar or radial configuration [7] (as shown in Figure 3.4) [2]. In a bipolar configuration, where LC molecules align themselves parallel to the LC interface, an optical texture with two points defects with opposite directions can be viewed under crossed polarizers. As a contrast, LC molecules in a radial configuration orient perpendicularly at the LC interface with strong anchoring strength. When under crossed polarizers, a single point defect can be observed at the center of the droplet. This characteristic optical property of LC emulsions has been widely applied to applied in biological and chemical sensing applications.

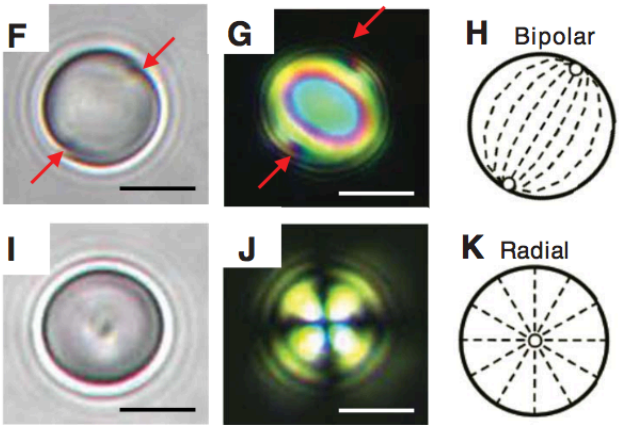

Fig. 3.4 (**H**) Schematic illustration of bipolar configuration of LC droplet. (**F**) Bright-field and (**G**) Polarized light microscopic image of LC droplet with a bipolar configuration. (**K**) Schematic illustration of radial configuration of LC droplet. (**I**) Bright-field and (**J**) Polarized light microscopic image of LC droplet with a radial configuration in ref. [2].

3.2 Adsorption of Surfactants at the Nematic Liquid Crystal Interface

For technological applications, LC-in-water emulsions must be stabilized against droplet coalescence by the addition of surfactants, nonpolar liquids, or water-immiscible polymers. A number of investigations have focused on the adsorption of surfactants at the aqueous-LC interface [14-17] Past studies have reported on the influence of surfactants on the orientation of LC molecules at the LC-water interface by using emulsions of LCs. However, the complex geometry of emulsions makes interpretation of the orientation of LC less obvious than when using a planar interface [14]. When a droplet of a nematic liquid crystal is present on the surface of water, it will spread spontaneously into a thin film with an obvious optical texture (Schlieren texture, four dark brush structure) corresponding to planar anchoring at the LC-water interface as shown in Figure 3.5(A). However, the introduction of surfactant sodium dodecyl sulfate (SDS) in the water phase

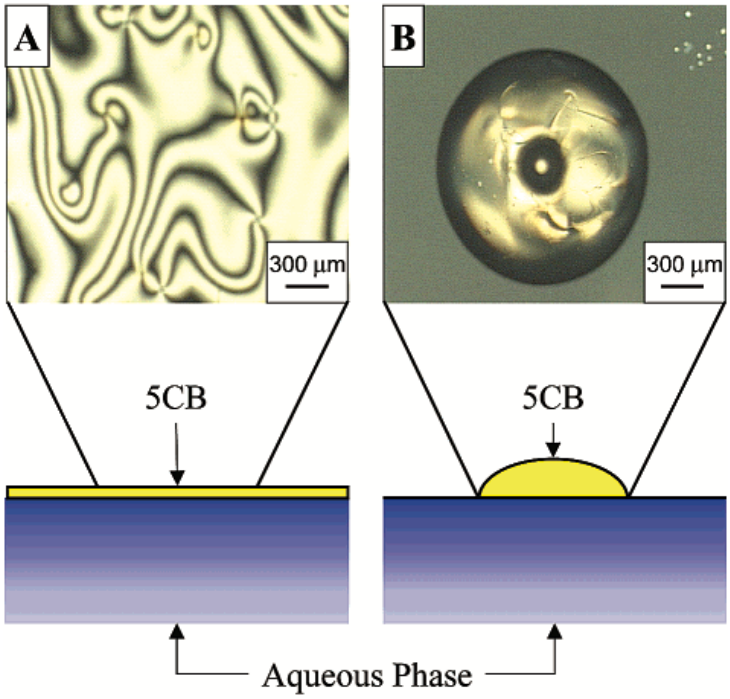

Figure 3.5 Optical images of 5CB deposited onto the surface of (A) water and (B) water containing 10mM SDS in ref. [14].

resulted in the 5CB thin film coalescing into droplets as shown in Figure 3.5(B), which makes interpretation of the molecular anchoring complicated. Brake and Abbott [14] presented an experimental system to study the adsorption of surfactants at the LC interface by confining the LCs into a copper grid as shown in Figure 3.6. A liquid crystal that has been studied is 4-pentyl-4-cyanobiphenyl (5CB). The nematic-isotropic temperature for 5CB is 35.2°C. The experiment was conducted at a temperature where 5CB remains a nematic phase. The 5CB was placed onto a microscopy copper grid, supported on a glass microscope slide treated with octadecyltrichorlosilane (OTS) as shown in Figure 3.6. OTS can induce a homeotropic anchoring of LC molecules, which are in close contact with OTS. Immersion of this optical cell into the aqueous phase of interest leads to the formation of stable interfaces between the aqueous phase and liquid crystal. In the absence of a surfactant, the orientation of 5CB molecules at the water-LC interface is parallel to the interface (planar anchoring). This orientation appears bright with a four-dark brush structure when viewed under microscopy with crossed polarizers as shown in Figure 3.6(B). Brake and Abbott [14] added surfactant SDS to the water, which results in the optical appearance change of 5CB from bright to dark under crossed polarizers as shown in Figure 3.6(C) [15]. The dark optical appearance of the LC texture is consistent with that of homeotropic anchoring. And they also found out the adsorption process of surfactants is reversible.

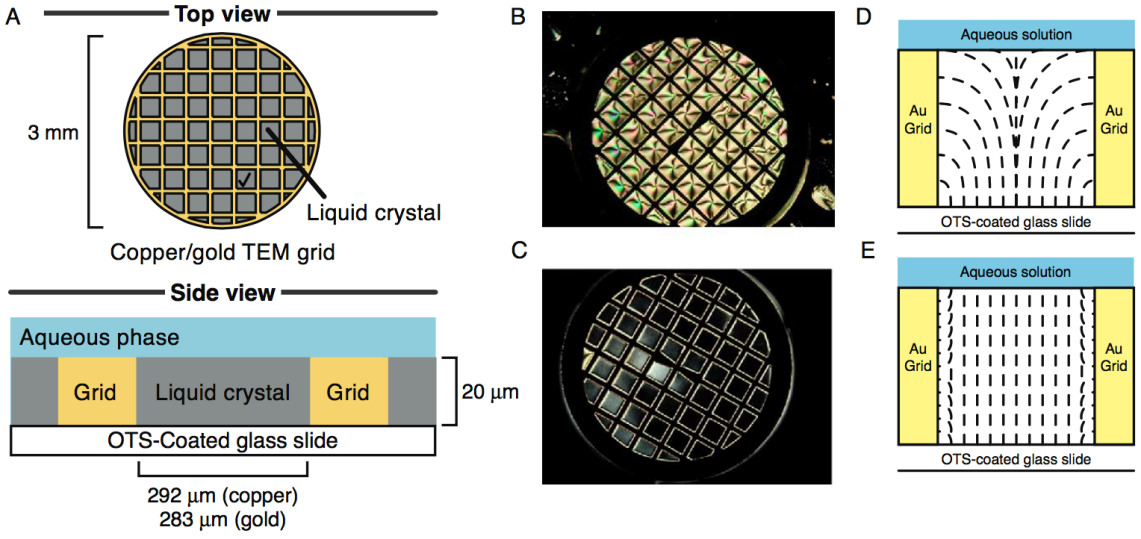

Figure. 3.6 A) Experimental geometry used to form stable interfaces between aqueous phases and thermotropic liquid crystals to study the self-assembly of amphiphiles. Top and side views

are shown. **B – C)** Optical images (crossed polarizers) of 5CB confined to a copper grid with a spacing of 292 μm that was supported on an OTS-coated glass slide and immersed under pure water (**B**) or an aqueous solution of 2.2 mM SDS (**C**). **D – E)** Schematic illustrations of the director profiles of the liquid crystal corresponding to planar anchoring of the liquid crystal at the interface with the aqueous phase (**D**) and homeotropic anchoring (**E**). Note that the orientation of the 5CB at the grid surface is normal to the grid-5CB interface in ref. [15].

In subsequent work, they used the same experimental system to study the effect of surfactant structure on the orientation of LCs at the water-LC interface [17]. They compared the influence of a series of surfactants with different structures as shown in Figure 3.7 to establish a standard for surfactants that give rise to specific orientations of LCs at the LC-water interface. They concluded that the orientation of LC molecules is largely determined by the structure of the hydrophobic moiety of the adsorbed surfactants, whereas the hydrophilic head does not influence orientational order. Bolaform surfactants adopting a looped configuration at the 5CB-water interface give rise to a planar orientation of LCs; long-chain surfactants with a tilted configuration preferentially align the LC molecules perpendicular to the interface (homeotropic alignment). SDS is a conventional anionic surfactant with one hydrophilic headgroup and one long chain hydrophobic tail. Surfactants with this type of structure usually adopt tilted configuration at the interface as shown in Figure 3.7(C). In contrast, bolaform surfactants are amphiphilic molecules that have hydrophilic groups at both ends of a sufficiently long hydrophobic hydrocarbon chain as shown in Figure 3.7(B).

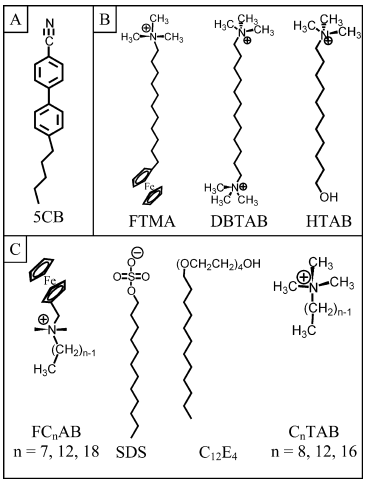

Figure 3.7 (**A**) Chemical structure of 5CB. (**B**) Chemical structures of surfactants that adopt looped configurations at air-water/oil-water interfaces. (**C**) Chemical structures of surfactants that adopt tilted configurations at air-water/oil-water interfaces in ref. [17].

Recent computational work [18] shows that liquid crystal 5CB can be used to impart order to interfacial arrangement of surfactants at the LC-water interface. When LC is confined to small droplets, LC can induce the formation of ordered domains where surfactants prefer to localize at the interface. This discovery is in contrast to past studies, which have well demonstrated the effects that surfactants have on the long-range orientation of liquid crystals. The liquid crystal is confined to nanodroplets, the interfaces of which are decorated with surfactant molecules. The surfactants induce the local perpendicular orientation of mesogens within the droplet. In the absence of surfactants, LC molecules at the interface align themselves parallel to the LC-water interface. LC molecules undergo a phase transition from a disordered isotropic phase to an ordered nematic or smectic LC phase. During this process, mesogens within the droplets will cause a transition of surfactants at the LC-water interface, resulting in the formation of a new ordered nanophase of surfactants at the LC-water interface as shown in Figure 3.8. This prediction offers a new approach for hierarchical assembly of structured materials.

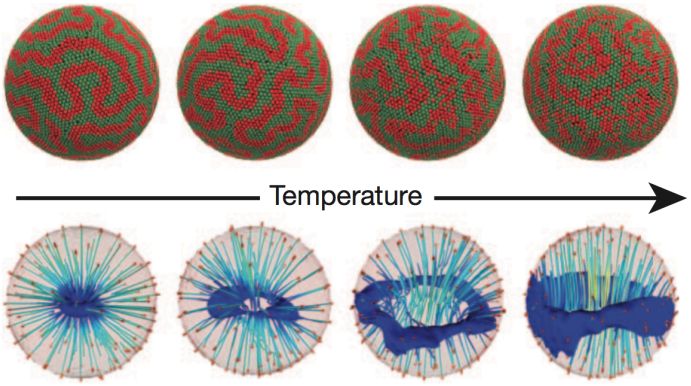

Figure 3.8. Director contour lines and defect core as a function of temperature, corresponding to a surfactant concentration of x_{surf} =0.5. The four temperatures shown here are T* = 2, 5, 10 and 11, respectively. At T*= 2, a smectic phase is observed. All other temperatures correspond to a nematic phase. As the temperature is lowered, the defect becomes increasingly localized at the center of the droplet and squeezes the director until the overall configuration of the LC is radial. Ordering of surface particles becomes increasingly pronounced as the temperature is reduced and the LC becomes more ordered in ref. [18].

3.3 Adsorption of Nanoparticles at Nematic Liquid Crystal Interface

Like surfactants, colloidal nanoparticles also adsorb at liquid-liquid interfaces, stabilizing emulsions. It is well known that the interfacial attachment of nanoparticles can be much stronger than that of surfactants, resulting in water-in-oil or oil-in-water emulsions of exceptional stability [19,20]. Nanoparticle-stabilized emulsions have been widely applied in a various fields including but not limited to food science, biomedicine, sensing, and catalysis [20-26] Their application to emulsions involving LCs, however, is only now beginning to receive more attention [22,23]. Considerable previous research has been focused on the various defects of LCs caused by the intrusion of colloid particles [35-40]. Nematic LCs exhibit orientational order along a unit direction, so-called director. However, LCs also adopts some morphological defects, where the director direction of LC molecules is ambiguous. The alignment of nematic LC molecules and corresponding defects can be easily disturbed by any introducing particles. The structure of the director filed around a particle is dependent on the interaction between the particle and LCs, which is usually referred to as anchoring. Particles that adopt planar anchoring will induce quadrupolar symmetry with two defects on the

surface, which are usually referred to as “boojums” [35]. In contrast, particles with homeotropic anchoring will induce either dipolar symmetry with point defects, or induce quadrupolar symmetry with Saturn-ring defects, as shown in Figure 3.9.

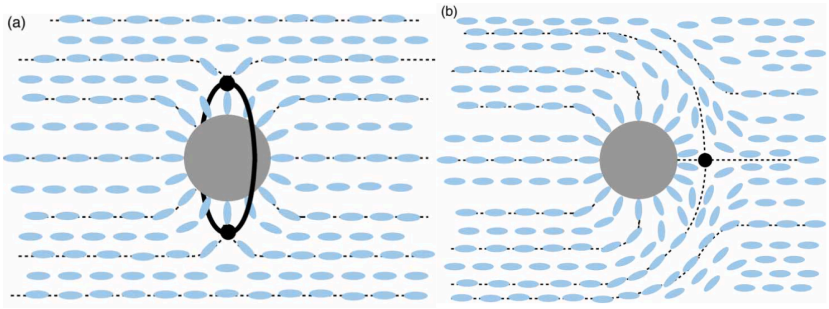

Figure 3.9 Two possible defects observed when a colloid with homeotropic anchoring on its surface, is embedded in a nematic liquid crystal. (a) For weak anchoring, a “Saturn ring” (the black circle) embraces the particle. This disclination pattern is associated with a quadrupolar symmetry of the director field. (b) For strong anchoring a satellite defect of charge −1, a hyperbolic hedgehog, accompanies the particle in ref. [35].

Recent computational work by Rahimi *et al.* [22] predicted that planar nanoparticles adsorb at the interface of bipolar LC droplets following a hexagonal arrangement as shown in Figure 3.10. They found out that the bipolar LC droplets with two boojums defects could be used to drive assembly of planar particles to the poles where defects exist and create dipolar defects. The intrusion of particles at the poles eliminates the high splay elastic energy and reduces the free energy. Particles adsorbed at the poles form into different packing arrangements that can be mapped onto hexagonal lattices. Among all these different packing arrangements, the one that covers the larger fraction of the surface area around the pole is the most stable and exhibits the lowest free energy.

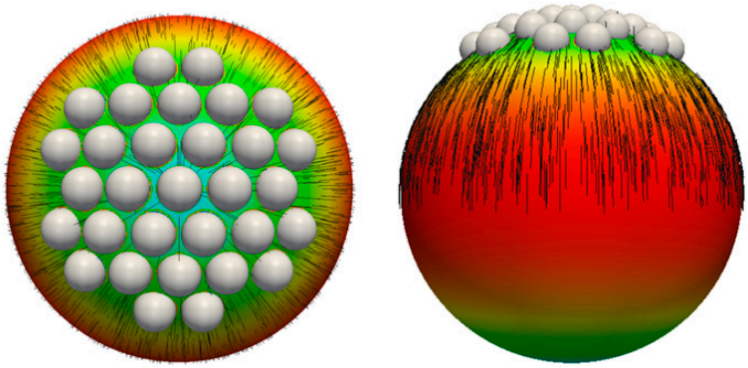

Figure 3.10. Hexagonal lattices arrangement of multi-particle at the pole of bipolar droplet, which covers the pole in ref. [22].

Experimental work done by X.Wang et al. [23] demonstrated the formation of organized assemblies of 1μm-in-diameter polystyrene colloids at the poles of nematic liquid crystal 5CB droplets (diameter 7-20μm) dispersed into water phase. For 5CB droplets decorated with PS particles, they reported 32 distinct arrangements of particles to form at the boojums or bipolar droplet configurations. All these different configurations (a ring consisting of five polystyrene particles) could be mapped onto a local hexagonal lattice as shown in Figure 3.11. This work provides further insight into the origin of such an arrangement. For colloidal particles already attached to the interface, the formation of hexagonal arrays in the vicinity of surface defects in the bipolar configuration (i.e., "boojums") is explained as the consequence of three key interactions: (i) splay attraction (a long-range attraction between the adsorbed particles at the interface and the boojums due to the increasing rate of strain (splay) of LC near the boojums, (ii) an attractive inter-colloid quadrupole-quadrupole elastic interaction, and (iii) interparticle electrostatic repulsion between colloids attached to the interface. The extent to which these interactions may influence the dynamics of self-assembly of nanoparticles at the LC-water interface is presently unknown.

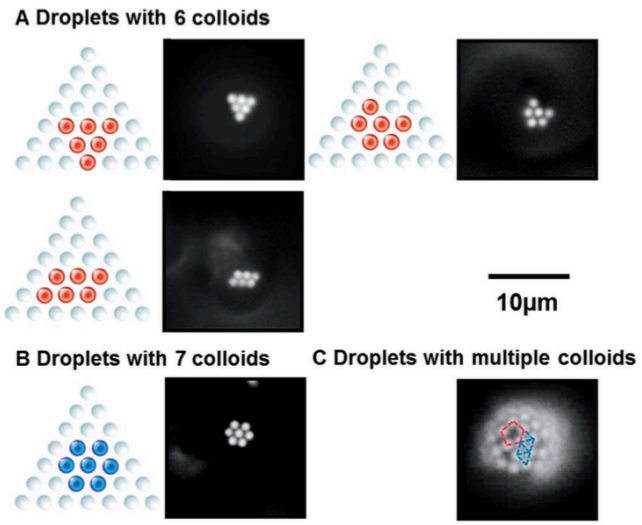

Figure 3.11. Packing arrangements most frequently observed for bipolar 5CB droplets with (A) six or (B) seven PS colloids adsorbed to their poles. (C) Packing arrangements observed for multiple PS colloids adsorbed at the surfaces of bipolar 5CB droplets. Colloids that follow a hexagonal or pentagonal arrangement are marked by blue or red dashed lines, respectively. In fluo-micrographs, the contrast is enhanced to highlight the arrangements of colloids in ref. [23].

3.4 Bizmark's Model for Irreversible Adsorption of Nanoparticles

The adsorption of spherical particles on interfaces (water-air or water-oil), is thermodynamically favored due to the reduction of surface or interfacial tension. The magnitude of the reduction in free energy, $|\Delta E|$, associated with the transfer of a spherical particle from the bulk phase to the fluid-fluid interface is given by the following equation [19]:

$$|\Delta E| = \gamma_0 \pi r^2 \left(1 - |\cos\theta|\right)^2 \tag{1}$$

where r is the radius of the particle, γ_0 is the interfacial tension of the pristine fluid-fluid interface and θ is the contact angle of a particle at the fluid interface measured through the aqueous phase. Unlike the case of surfactants, the adsorption energy of particles can exceed the mean energy of thermal fluctuations by several orders of magnitude, which indicates that the adsorption process of solid particles is effectively irreversible. An

alternative approach to Equation (1) for estimating the adsorption energy is suggested on the basis of simple thermodynamic arguments [25]:

$$\left|\Delta E\right| = \frac{\gamma_0 - \gamma_\infty}{\Theta_\infty}\pi r^2 \tag{2}$$

In Equation (2), γ_∞ and Θ_∞ are the interfacial tension and fractional coverage of the interface at steady state, respectively. The surface coverage has been approximated by the greatest possible coverage of the interface, a value of $\Theta_\infty = 0.91$, which corresponds to the hexagonal close packing of particles at the interface. Equation (2) demonstrates that the reduction of γ is directly related to the binding energy of the particles in the absence of particle-particle interactions. The binding energy, $\left|\Delta E\right|$, can be directly calculated from the experimental measurements if the surface coverage of particles at the interface is known previously. The simulation study [41] also predicts $\Theta_\infty = 0.91$ for irreversible adsorption of nanoparticles.

A newly formed interface of a surfactant solution has an initial surface tension, γ, which is very close to the surface tension of the solvent, γ_0. After a period of time, surface tension γ will decrease to the equilibrium value, γ_∞, because of the self-assembly of surfactants at the interface. This dynamic surface (interfacial) tension (DST or $\gamma(t)$) is an important property for many important industrial and biological processes and has been used to study the dynamic adsorption of surfactants in terms of the classic model of Ward and Tordai [42]. To date, the classic model of Ward and Tordai has been applied to probe quantitatively the dynamics of nanoparticle adsorption. This approach provides a suitable model to connect dynamic surface (interfacial tension) to transient coverage of the interface of nanoparticles when adsorption is reversible. The following asymptotic equations have been applied to interpret data from the early ($t \to 0:$) and the late ($t \to \infty:$) stages of nanoparticle adsorption:

$$t \to 0: \quad \gamma = \gamma_0 - 2RTC_0\sqrt{\frac{Dt}{\pi}} \tag{10}$$

$$t \to \infty: \quad \gamma = \gamma_{\infty} + \frac{RT\Gamma_{\infty}^{2}}{C_0}\sqrt{\frac{\pi}{4Dt}} \tag{11}$$

in which R is the gas constant, T is the temperature, C_0 is the molar bulk concentration, Γ_{∞} is the molar adsorption density at steady state, and D is the nanoparticle diffusion coefficient. However, a critical flaw exists with the application of classic equation 3 to DST data from irreversible adsorption of nanoparticles (when $|\Delta E| \gg k_B T$). For the condition that is $|\Delta E| \gg k_B T$, estimations of nanoparticle coefficient D by equation 3 ($D_{t\to 0} \gg D_{t\to\infty}$) and equation 4 ($D_{t\to\infty}$) have shown that $D_{t\to 0} \gg D_{t\to\infty}$, which grossly overestimate the diffusion coefficient D. The estimations of diffusion coefficient D from equation 3 and 4 show great odds with theoretical expectations and physical understanding. The failure of the classic model of Ward and Tordai to analyze the irreversible adsorption of nanoparticles has been demonstrated by Bizmark et al. [26] In order to analyze the dynamics of the adsorption process of nanoparticles, Bizmark et. al presented another approach to probe the kinetics of irreversible adsorption and self-assembly of nanoparticles at the air-water interface as shown below:

$$t \to 0: \quad \gamma = \gamma_0 - 2N_A|\Delta E|C_0\sqrt{\frac{Dt}{\pi}} \tag{3}$$

$$t \to \infty: \quad \gamma = \gamma_{\infty} + \frac{K_l|\Delta E|}{\left(\pi r^2\right)^2 N_A C_0}\sqrt{\frac{1}{Dt}} \tag{4}$$

In their approach, they consider a planar interface, because the size of the nanoparticle they used is much smaller than the droplet size. Then they choose a coordinate system with the x-axis perpendicular to and directed toward the solution. They developed a material balance for the adsorbed nanoparticles the interface ($x = 0$) as follows:

$$\frac{d\Theta}{dt} = -N_A S_j\Big|_{x\to 0^+} \tag{12}$$

where Θ is the surface coverage of nanoparticles adsorbed at the interface, j is the molar flux of nanoparticles, N_A is Avogadro's number, and S is the occupied surface (interface) area by a single nanoparticle. For early stages ($t \to 0$) in adsorption process, the adsorption flux can be described by Fick's law:

$$j\Big|_{x\to 0^+} = -D\frac{\partial C}{\partial x}\Big|_{x\to 0^+} = -C_0\sqrt{\frac{D}{\pi t}} \tag{13}$$

In equation (13), $C(x,t)$ is the solution to a simple one-dimensional transient diffusion problem [43]. Substituting equation (13) into equation (12) and integrating gives:

$$\Theta = 2\pi r^2 N_A C_0\sqrt{\frac{Dt}{\pi}} \tag{14}$$

Equation (2) can be generalized to connect surface coverage and surface (interfacial) tension at any time. Apply equation (14) to equation (13), they obtain:

$$\gamma = \gamma_0 - \frac{\Theta}{\pi r^2}|\Delta E| \tag{15}$$

The item Θ can be eliminated between equation (14) and (15), to yield the novel equation (4) which can be used to describe the early stages of dynamic adsorption of nanoparticles.

$$\gamma = \gamma_0 - 2N_A|\Delta E|C_0\sqrt{\frac{Dt}{\pi}} \tag{4}$$

It is obvious that when $|\Delta E| = k_B T$ equation (4) is exactly same as equation (10). The early time DST data can be alternatively analyzed in terms of equation (4). In this equation, the diffusion coefficient is directly calculated from Stokes-Einstein equation ($D = k_B T/6\pi\mu r$). Then the adsorption energy, $|\Delta E|$, can be estimated from the slope of linear regression of early time DST data against $\sqrt{t}$.

For the later stages of adsorption of nanoparticles, as nanoparticles keep adsorbing onto the interface, the interface gets close to maximum coverage. The already absorbed nanoparticles will hinder the adsorption of nanoparticles, resulting in smaller adsorption flux than that predicted by equation (13). Besides the energy ϕ of some specific physicochemical interactions between the interface and adsorbing particles, such as Van der Waals, hydrophobic and electrostatic forces, another new energy ϕ_s associated with the interaction between the adsorbing particle and already adsorbed particles. The equation quantifies the energy between the adsorbing particle and already adsorbed particles is as follows [44]:

$$\phi_s = -k_B \ln \overline{B}(\Theta) \tag{16}$$

$\overline{B}(\Theta)$ is so-called the generalized blocking function. Then the particle flux during the later stages of irreversible adsorption is described as follows:

$$j\Big|_{x\to 0^+} = k_a N_A C_0 \overline{B}(\Theta) \tag{17}$$

in which k_a is the adsorption constant, which ϕ is also a function of diffusion coefficient and specific interaction energy, but is not relative to $\overline{B}(\Theta)$. Then the material balance for absorbed particles at the interface is as follows [44]:

$$\frac{d\Theta}{d\tau} = k_a N_A C_0 S \overline{B}(\Theta) \tag{18}$$

Equation (18) can be expressed in terms of non-dimensional parameters ($\overline{k}_a \equiv k_a(L/D)$, $\tau \equiv tD/L^2$, and $L \equiv 1/(N_A C_0 S)$) as follows:

$$\frac{d\Theta}{d\tau} = \overline{k}_a \overline{B}(\Theta) \tag{19}$$

When surface coverage approaches $\Theta_{\max}$, the generalized blocking function can be approximated as $\overline{B}(\Theta) \cong 2.32(1-\Theta/\Theta_{\max})^m$, where m equals to 3 for monodisperse spheres. When this approximation applied to equation (19) and the result is integrated, the following is obtained:

$$\Theta = \Theta_{\max} - \frac{K_l}{\sqrt{t}} \tag{20}$$

where $K_l = \Theta_{\max}(\Theta_{\max}/4.64k_a)^{1/2}$. Applying the definition of the dimensionless time (t) to equation 15, results in:

$$\Theta = \Theta_{\max} - \frac{K_l}{\sqrt{(\pi r^2 N_A C_0)^2 Dt}} \tag{21}$$

In the end, elimination Θ of between equation (15) and (21), gives the result as below:

$$\gamma = \gamma_\infty + \frac{K_l |\Delta E|}{(\pi r^2)^2 N_A C_0}\sqrt{\frac{1}{Dt}} \tag{4}$$

The surface tensions of liquid crystal have been measured by a variety of

techniques, such as the Wilhelmy plate method, maximum bubble pressure and pendant drop method. The surface (interfacial) tension of nematic LCs is expected to strongly rely on the alignment of the LC molecules at the interface and LCs possess large viscosity. As a result, the pendant drop method is considered as the most suitable one for measurements of interfacial tension of nematic LCs. This method has several advantages compared to other methods [45,46]:

a) The interfacial tension values obtained are independent of the contact angle;
b) The viscous drag of the liquid crystal has no effects on the measurement, because it is a static method;
c) The area of the LC drop that is in direct touch with another solid surface (besides the isotropic phase of interest) is very small, so wall effects have less effect on the experimental results.
d) This method requires a smaller amount of liquid crystal.

The pendant drop method has been used to measure the surface or interfacial tension of nematic LCs in many studies [16,45-48]. This method [45] has been used to measure the surface tension of some nematic liquid crystals (p-azoxyanisole, p-anisaldazine, and p-methoxy benzylidene-p'-n-butylaniline) in order to study the temperature dependence of surface tension. They found that the slope in nematic phase is initially negative but changes sign near the nematic-isotropic transition temperature. Tarkhan [46] measured the surface tension of 5CB liquid crystal in a wide temperature range at the free and 5CB/glycerine interface. Kim et al. [16] used the pendant drop method to measure the interfacial tension of a nematic liquid crystal in water with homeotropic surface alignment to study the temperature dependence near nematic-isotropic temperature T_{NI} of interfacial tension of 5CB. They used surfactant cetylyrimethylammonium bromide (CTAB), which is known to induce a transition in liquid crystal surface alignment from planar to homeotropic, to reduce the interfacial tension values. They pointed out that there exist some discrepancies of the density of the liquid crystal 5CB in the previously published results [47,48]. Tintaru et al. [47] measured the temperature dependence of surface tension by pendant drop method for four

compounds from the homologous series of alkylcyanobiphenyls (nCB). They proposed a linear regression to calculate the density of nCB:

$$\rho = A + B\left(T - T_{NI}\right) \tag{22}$$

For 5CB at its nematic phase $A = 1.0239$ and $B = -1.243\times10^{-3}$; for isotropic phase, $A = 1.0214$ and $B = -0.866\times10^{-3}$.

3.5 Pendant Drop Tensiometry

In this work, the surface or interfacial tension is measured by pendant drop tensiometry. Figure 3.12(a) is a schematic image of a pendant drop tensiometer. Generally, a drop with certain volume is formed at the tip of a syringe by a motorized syringe pump. The cuvette is filled with another liquid phase of interest. Images of the drop are captured by a high quality CCD camera and then this shape is fitted to a model equation of its profile as shown in Figure 3.12(b).

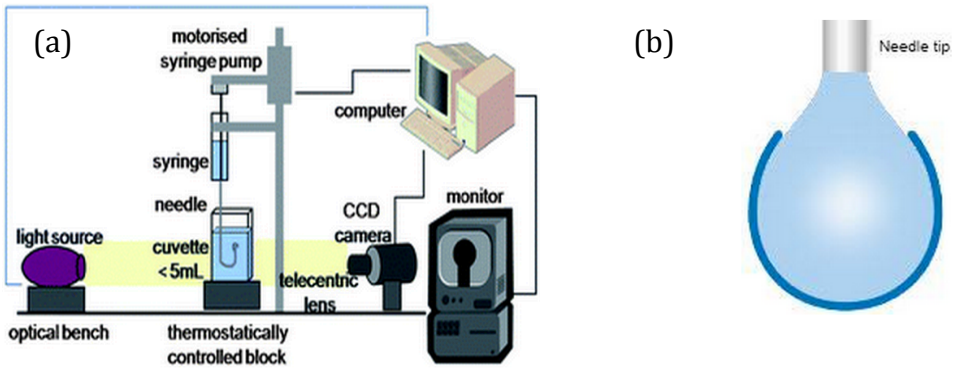

Figure 3.12 (a) Schematic image of pendant drop tensiometer in ref. [63]; (b) schematic image the fitting of Laplace-young equation to a drop profile in ref. [64].

The shape of liquid drops can be described by the well-known Laplace-Young equation, which is given by:

$$\Delta p = -\gamma \nabla \cdot \hat{n} = \gamma \left(\frac{1}{R_1} + \frac{1}{R_2} \right) \tag{23}$$

where Δp is the pressure difference across the fluid-fluid interface, γ is the surface or interfacial tension, $\hat{n}$ is the unit normal pointing out from the surface, R_1 and R_2 are the principal radii of curvature. Laplace-Young equation is just a balance between gravity, surface tension and hydrostatic pressure. When the drops are axisymmetric, the Laplace-Young equation can be written as [49]:

$$\left(\frac{1}{R_1} + \frac{1}{R_2} \right) = -\frac{\Delta \rho g y}{\gamma} + f\left(R_0\right) \tag{24}$$

where $\Delta \rho$ is the density difference of two fluids, g is the gravitational acceleration and R_0 is radius of curvature at $y = 0$ (shown in Figure 3.13); the term $\left(1/R_1 + 1/R_2\right)$ is the mean curvature of the drop; this curvature is a function of the y position can be expressed using following differential geometry [49]:

$$\left(\frac{1}{R_1} + \frac{1}{R_2} \right) = \frac{d^2 y / dx^2}{\left[1 + \left(dy/dx\right)^2\right]^{3/2}} + \frac{dy/dx}{x\left[1 + \left(dy/dx\right)^2\right]^{1/2}} \tag{25}$$

Solutions to the Laplace-Young equation provide the variation of the curvature as a function of elevation. The mean curvature of the pendant drop versus the y position, and the slope of the best straight line through data are obtained. With the knowledge of the density difference between two fluids and position y, surface interfacial tension can be calculated.

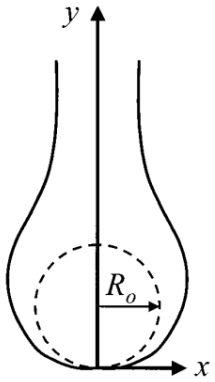

Figure 3.13 Pendant drop showing the geometrical variables in ref. [44].

The pendant drop tensiometer measurement becomes inaccurate when the dimensionless ratio between gravitational and interfacial forces is small, that is, Bond number is low (<0.1). The bond number is defined as:

$$Bo = \frac{\Delta\rho g\left(R_0\right)^2}{\gamma} \qquad (26)$$

where $\Delta\rho$ is the density difference, g is the gravitational acceleration, γ is the interfacial tension, and R_0 is the radius of curvature at the drop apex. The value of Bo should be lie within the range from approximately ~0.1-0.6 in order for the mentioned procedure to be valid [16]. A small Bond number indicates that interfacial forces dominate the gravitational forces.

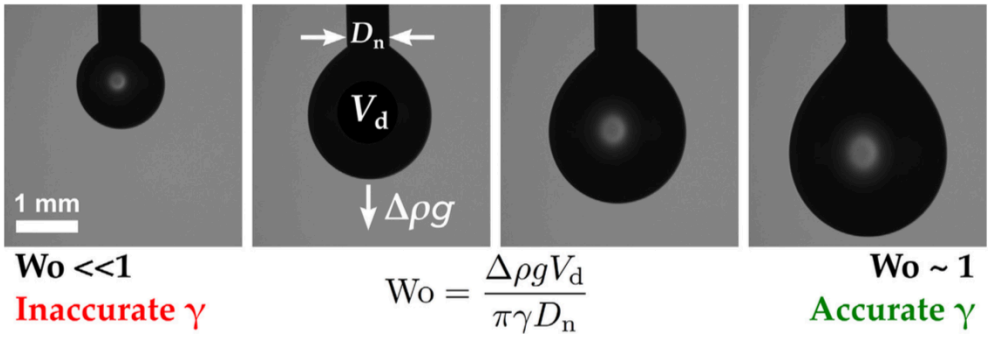

Figure 3.14. Illustrations of drop profiles showing the geometrical variables in ref. [28].

The reliability of the interfacial tension measurements depends on how accurately the Bond number can be determined from each particular experimental system. However, the Bond number is usually unknown prior to the interfacial tension measurements. The density difference between liquid crystal 5CB and water is also very small. Instead, another dimensionless number, so-called Worthington number (Wo) [28], is considered as a better guide to characterize the precision of IFT results using a pendant drop tensiometer in the case of a small Bo number is small. Wo number is given by:

$$Wo = \frac{\Delta\rho g V_d}{\pi\gamma D_n} \tag{27}$$

In this equation, $\Delta\rho$ is the density difference between two phases, g is the gravity acceleration, γ is the interfacial tension, V_d is the volume of the droplet, and D_n is the diameter of the syringe tip as shown in Figure 3.14. The Wo number scales from 0 to 1 [28]. The closer Wo is to 1, the more accurate is the interfacial tension measurement.

3.6 Polarized Optical Microscopy

The polarizing microscope has served as the primary method of determining the alignment properties of liquid crystals. A typical setup of a polarizing microscope is shown in Figure 3.15. Generally, it consists of five main parts: light source, two polarizers, ocular (eyepiece), objectives and a rotation stage. The light source is usually a halogen light bulb emitting white light. Nematic liquid crystals are uniaxially birefringent, i.e. it has a higher refractive index, n_e, in the direction parallel to the nematic director. If a nematic liquid crystal is placed between two crossed polarizers with the light passing through the n_e direction, the nematic LCs will induce a phase shift in the light, resulting in a bright appearance on a dark background. When the local director field is oriented parallel to either of the polarizers, no light phase shift occurs, resulting in a totally dark appearance with crossed polarizers. For LC molecules confined to a nematic droplet, such as bipolar or radial droplets, different textures of LCs can be observed as shown in Figure 3.4 with two crossed polarizers [29]. The different patterns correspond to different molecular alignments of LCs at the interface.

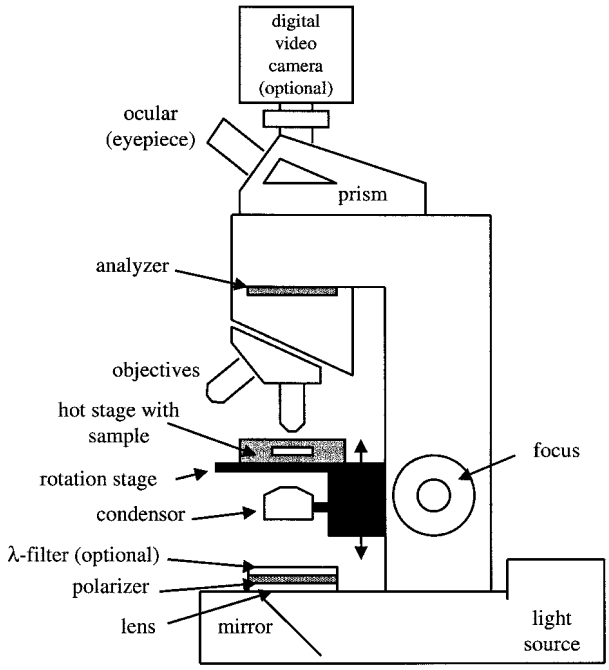

Figure 3.15 Schematic setup of a polarizing microscope used in texture studies and the optical behaviour of uniformly aligned liquid crystal phases in ref. [29].

Chapter 4

Experimental Section

4.1 Experimental Materials

Liquid crystal (LC) 4-cyano-4'-pentylbiphenyl (5CB) was directly purchased (product code: C1550-5g) from Tokyo Chemical Industry (TCI) and used as received. The structure of 5CB is shown in Figure 4.1. A value of 1.028 g cm^{-3} is taken for the density of 5CB at 22 °C reported by Dunmur and Miller [50], which compares very well with the value of 1.03 g cm^{-3} provided by the TCI company.

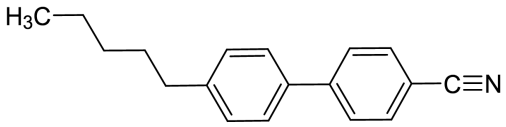

Figure 4.1. Schematic structure of nematic liquid crystal 5CB.

Aqueous colloidal suspensions of ethyl cellulose (EC) nanoparticles with an average hydrodynamic radius of 44nm were prepared following an anti-solvent

precipitation method described elsewhere [51]. First, a solution (10.7 g L-1) of EC (Sigma-Aldrich, product code: 247499-100G) in HPLC-grade isopropyl alcohol (IPA) (Caledon, product code: 8601-7) was prepared for later use. Then add an equal volume of ultrapure deionized (DI) water (~17 MΩcm) was added, resulting in a turbid solution due to the anti-solvent effect. Note that the mixture of water and isopropyl alcohol has an azeotropic point at 0.6813 mole fraction of IPA. Then the solution was boiled while stirring to concentrate the suspensions, until the composition of IPA present was less than 0.3%. The Figure 4.2 shows the steps of synthesis of EC nanoparticles. The colloidal suspension of EC nanoparticles used for later dynamic interfacial tension measurement is diluted to 0.3 g L^{-1} and 0.5 g L^{-1}.

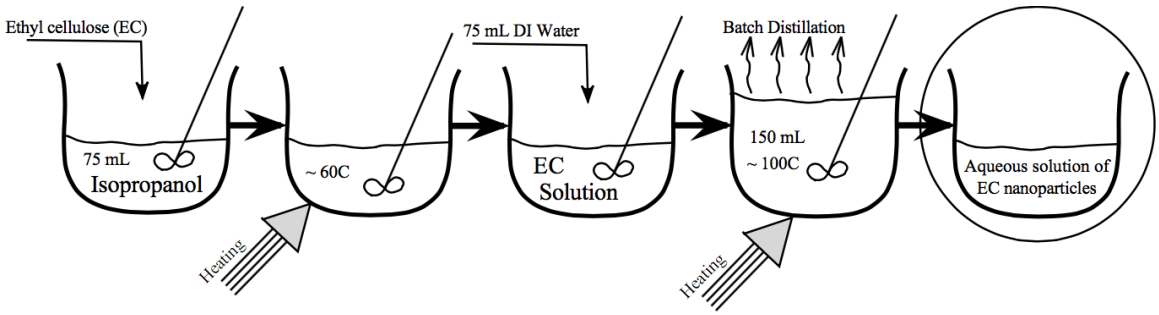

Figure 4.2 Illustration of steps of synthesis of EC nanoparticles suspension. This image is directly taken from University of Waterloo, Master Thesis, Navid Bizmark with permission.

4.2 Measurement of Dynamic Interfacial Tension

The surface and interfacial tensions of 5CB were determined (at 22 °C) by analyzing the profile of the axisymmetric drop shape using a pendant drop tensiometer (VCA 2500 XE, AST Products, Billerica, MA) and software employed in previous studies [26,52]. A schematic of pendant drop tensiometer is shown in Figure 4.3. A preset 5CB drop (15μL) was generated by a motorized syringe (20 gauge, 0.603 mm diameter) in a transparent glass cuvette filled with the suspension of EC nanoparticles. A high speed CCD camera was employed to capture images of the pendant drop at specified

frame rates. To capture the early stage of the adsorption (the first two minutes after the formation of the pendant drop), a frame rate of 12 images s^{-1} was used. For later stages of adsorption (up to 1 h), a frame rate of 6 images min^{-1} was chosen. The dynamic interfacial tension (IFT) of at least ten droplets was measured at two EC nanoparticle concentrations (i.e., 0.3 g L^{-1} and 0.5 g L^{-1}). Prior to any series of IFT measurement, the surface tension of ultrapure deionized (DI) water was measured. A value of 72.3±0.2 dyne cm^{-1} was consistently obtained at 295 K in agreement with the previous study[26] A surface tension of 34.5±0.4 dyne cm^{-1} was also measured for 5CB conforming to the reported values. With the same instrument used for tensiometry, we measured the contact angle of 5CB drops against air and water on glass slides spin-coated with a solution of 4 wt.% EC in ethanol at a speed of 2000 rpm for 25 s.

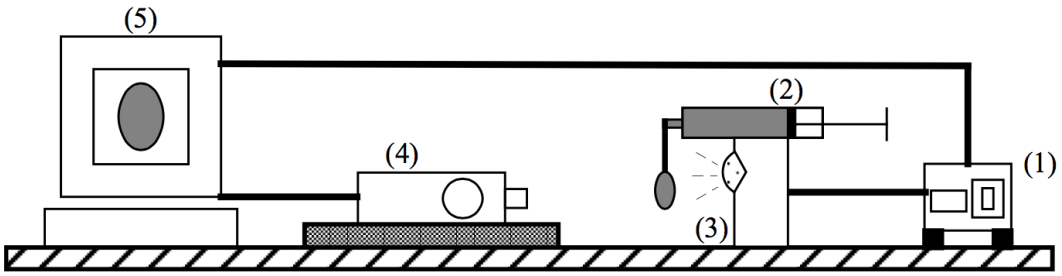

Figure 4.3 Illustration of the pendant drop tensiometer setup: (1) syringe controller, (2) micro syringe containing the colloidal solution, (3) light source, (4) high-speed CCD camera, and (5) computer. This image is directly taken from University of Waterloo, Master Thesis, Navid Bizmark with permission.

The shape of liquid drops can be described by the well-known Laplace-Young equation:

$$\Delta p = -\gamma \nabla \cdot \hat{n} = \gamma \left(\frac{1}{R_1} + \frac{1}{R_2} \right) \tag{28}$$

where Δp is the pressure difference across the fluid-fluid interface, γ is the surface or interfacial tension, $\hat{n}$ is the unit normal pointing out from the surface, R_1 and R_2 are the principal radii of curvature. The shape of the drop is the result of a balance between those forces. Those drop profiles are analyzed by Laplace-Young fitting as shown in Figure 4.4.

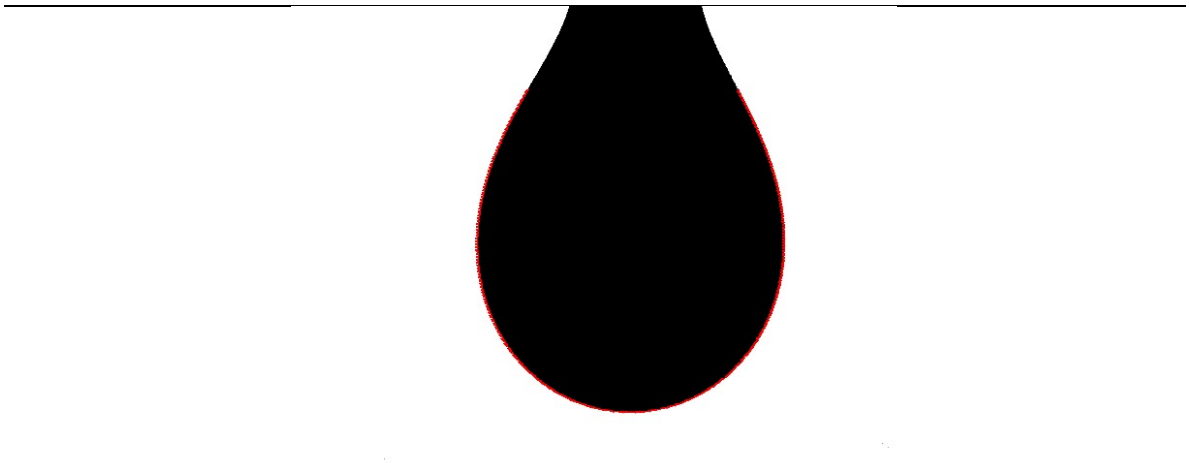

Figure 4.4 Fitting Laplace equation on the entire profile of a nematic liquid crystal 5CB droplet.

4.3 Measurement of Contact Angle

Contact angles of nematic liquid crystal 5CB in water and air are measured by pendant drop tensiometry. First of all, glass microscope slides are rinsed with water, ethanol, and methanol. Then they are dried under a stream of gaseous nitrogen. A 4wt% EC in ethanol solution is prepared by adding a given amount of EC solution (10g/L) into ethanol while continuously stirring and heating up to 50°C. Then cleaned glass slides are spin-coated with the 4wt% EC solution. Spin coating is a procedure applied to deposit uniform thin film onto the substrate. To do this, the cleaned glass substrate is placed onto the spinner's holder. And a small amount of 4wt% EC in ethanol solution is applied onto the substrate. The set-up of the spinner parameters is as follows:

Spin speed: 2000 RPM
Spin time: 25s
Accel time: 5s
Decel time: 5s

The spinner is turned on, and then the substrate is rotated at the set-up speed in order to spread the coating material by centrifugal force. Rotation is continued with the coating fluid spins off the edges of the glass substrate, and a uniform thin film is achieved. Figure 4.5 demonstrates the spinning coating process.

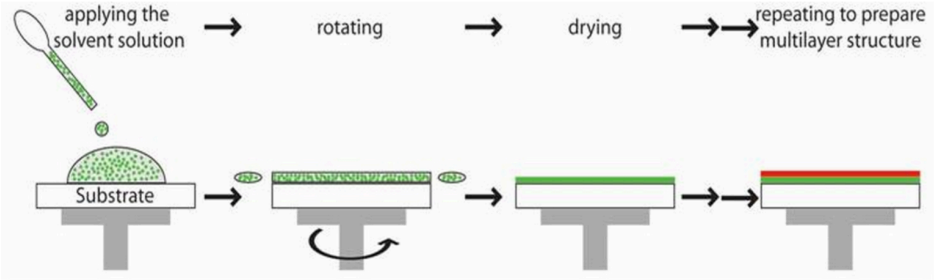

Figure 4.5 Illustration of spinning coating process in ref. [65].

To measure the contact angle, the EC-treated glass substrate immersed into water (or air). A small amount of nematic liquid crystal 5CB is dropped onto the EC-treated glass substrate. CCD camera is used to capture images of the 5CB drop in water (in air). The image is analyzed by the software, revealing information on the contact angles of 5CB in water and in air.

4.4 Optical Analysis of Liquid Crystal Textures by Polarized Optical Microscopy

The orientation of 5CB molecules was examined using an Axiovert 200 microscope with crossed polarizers. To this aim, minor modifications were made to the reported procedure [14] to prepare the optical cells. Briefly, liquid crystal samples were prepared between two EC spin-coated glass slides to make a sandwich-like cell. Orthoscopic examination were performed on the optical cells placed on a rotating stage between crossed polarizers with the source light intensity set to 50% of full illumination. Rotating the crossed polarizers, we determined homeotropic or planar alignments of the LC

molecules by observing no light transmission (black) or complete light transmission (bright), respectively, through the optical cells. Light transmission corresponds to planar anchoring of the 5CB molecules, while no light transmission is referred to as homeotropic alignments of the 5CB molecules [14,29] as shown in following Figure 4.6:

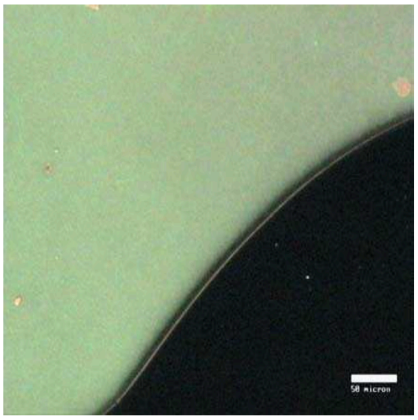

Figure 4.6 Demonstration of flow induced planar orientation (top left) on a substrate with homeotropic boundary conditions, prepared by deposition of a Langmuir Blodgett film. Only after considerable time has elapsed do homeotropic domains nucleate and grow (bottom right) in ref. [29].

Chapter 5

Results and Discussion

5.1 Dynamic IFT Measurement.

The goal of our initial experiments was to measure the dynamic interfacial tension (IFT) of 5CB in aqueous suspensions of EC nanoparticles by pendant drop tensiometry. Dynamic IFT of 5CB was measured in the presence of EC nanoparticles suspended in an aqueous phase at two different concentrations (0.3 g L^{-1} and 0.5 g L^{-1}). Figure 5.1 compares the equilibrium shapes of a pendant nematic liquid crystal 5CB drop suspended in water from the early time ($t \to 0$) and the late time ($t \to \infty$). Adsorption of EC nanoparticles at the interface reduces the IFT causing departure from the initially spherical shape of the drop.

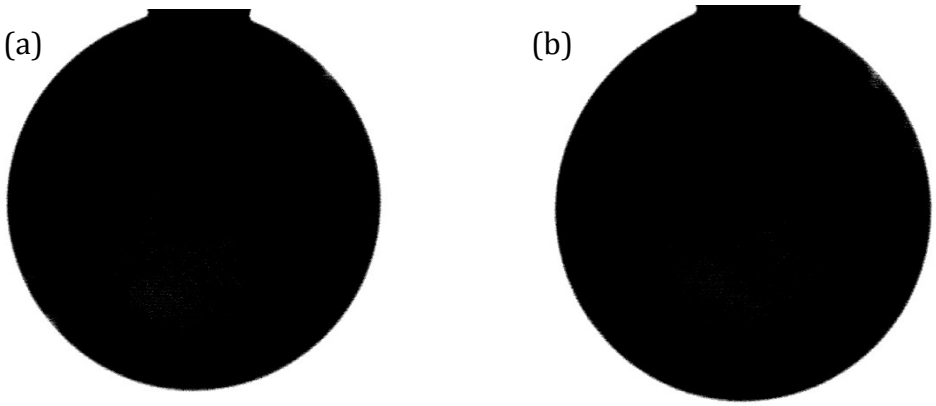

Figure 5.1 Difference in shape between pendant drop profile of nematic 5CB suspended in 0.5 g L^{-1} EC solution from (a) early time ($t \to 0$), regarded as EC-free water phase; (b) late time ($t \to \infty$).

Figure 5.2 compares the average dynamic IFT results of these two conditions showing a significant reduction in interfacial tension in either case. The interfacial tension of 5CB droplet in 0.5 g L^{-1} of EC nanoparticles solution drops faster. Pendant drop tensiometry is based on the analysis of the shape of the profile of the pendant drop of the suspended liquid. The drop shape profile is analyzed by Young-Laplace equation, which gives the interfacial tension from knowledge of the density difference $\Delta\rho$ between the two liquids at the temperature of measurement. Pendent drop tensiometry requires precise determination of density difference between the tow liquids. The density of water is 998 kg m^{-3} at 22 °C. A value of 1028 kg m^{-3} (at 22°C) is directly taken for the density of 5CB to analyze dynamic IFT data as shown in Figure 5.3. Deschamps et. al [53] presented the presenting linear correlation expressing the density of 5CB as a function of temperature as follows:

$$\rho(T)/kg\cdot m^{-3} = a_0 + a_1\left[(T - T_{NI})/K\right] \tag{29}$$

Here, a_0 and a_1 are parameters, T is the actual temperature, and T_{NI} is the temperature of the nematic-isotropic phase transition (clearing point). For liquid crystal 5CB in nematic phase, $a_0 = 1010.48$, $a_1 = -0.9230$ and $T_{NI} = 35.2°C$. The variation in density of 5CB from two studies leads to uncertainty of approximately 17% in the estimation of the density difference between 5CB and water. Because the interfacial tension is directly

proportional to density difference $\Delta\rho$, a 17% uncertainty of our IFT results.

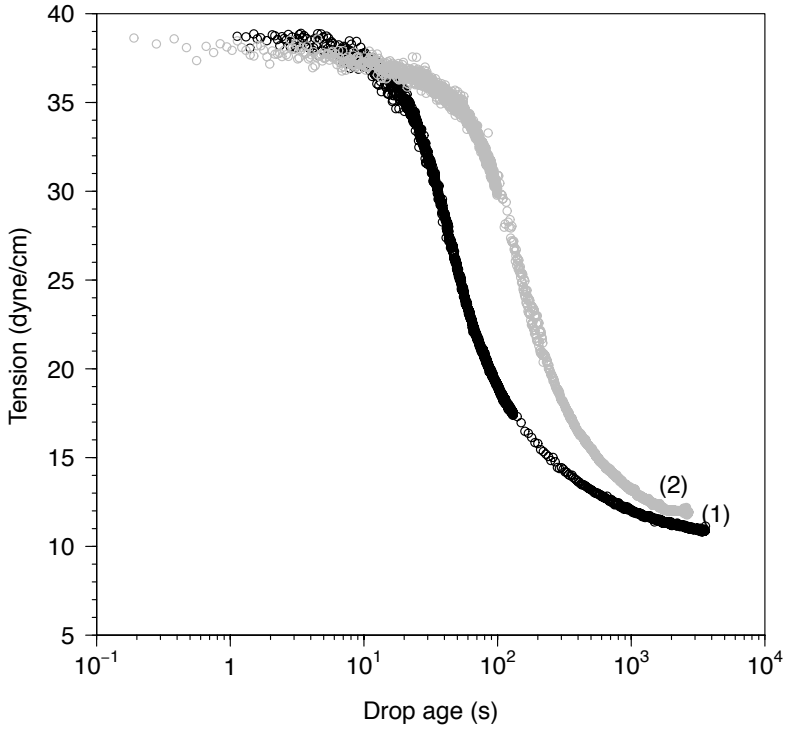

Figure 5.2 Dynamic interfacial tension (IFT) measurement of 5CB in EC nanoparticles with a concentration of (1) 0.5g L^{-1} and (2) 0.3g L^{-1}

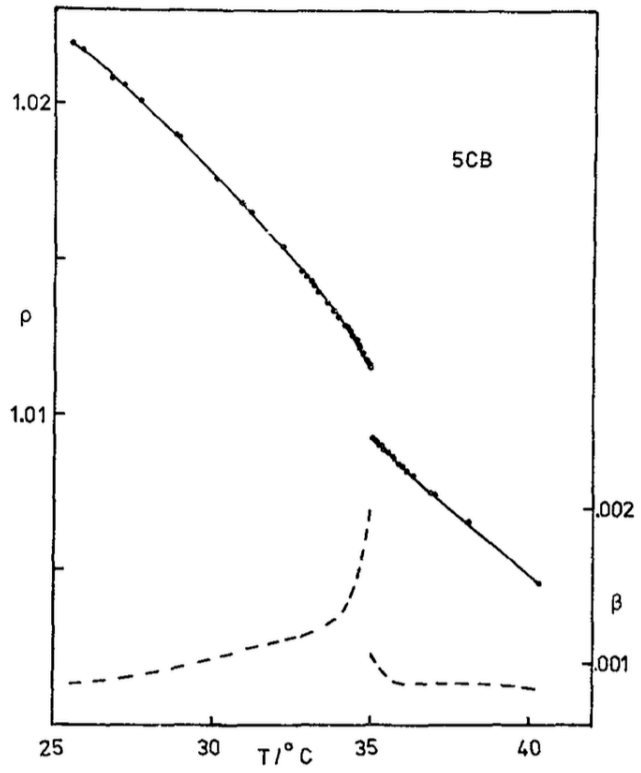

Figure 5.3 Temperature dependence of density of nematic liquid crystal 5CB reported by Dunmur et al in ref. [50].

Spherical pendant drops can be expected when the gravitational force is small compared to interfacial tension force, that is, when the Bond number is less than 0.1. Bond number is defined as a dimensionless ratio between gravitational force and interfacial tension, given by [16]:

$$Bo = \frac{\Delta\rho g\left(R_0\right)^2}{\gamma} \tag{26}$$

Here, $\Delta\rho$ is the density difference, g is gravitational acceleration, γ is the interfacial tension, and R_0 is the radius of curvature at the drop apex. Pendant drop tensiometer measurement is inaccurate when the Bond number is low (<0.1). A small Bond number indicates that interfacial forces dominate the gravitational forces. The reliability of the interfacial tension measurements depends on how accurately the Bond number can be determined for each particular experimental system. However, the Bond number is unknown prior to the IFT measurements. Instead, another dimensionless number, the so-

called Worthington number (Wo), is considered as a better guide to predict the precision of IFT results using a pendant drop tensiometry, and it is given by [28]:

$$Wo = \frac{\Delta\rho g V_d}{\pi\gamma D_n} \tag{27}$$

In which $\Delta\rho$ is the density difference between two phases, g is gravity acceleration, γ is the interfacial tension, V_d is the volume of the droplet, and D_n is the diameter of the syringe tip. Worthington numbers are calculated for both the early time and late time IFT data of 5CB drop in 0.3 g L^{-1} EC nanoparticles solution, which are 0.06 and 0.28 respectively. These values are obtained with 3% relative standard error (RSD) for the measurement from the early time and 1.8% RSD for the measurement at the late time, according to the analysis presented by Berry et al. Their results are summarized in Figure 5.4, which shows the percentage relative standard deviation (%RSD) for each measurement set as a function of wo. The surface tension of 5CB is also measured to be 34.3±0.92 dyne cm^{-1}, in good agreement with those reported in previous studies [1,54].

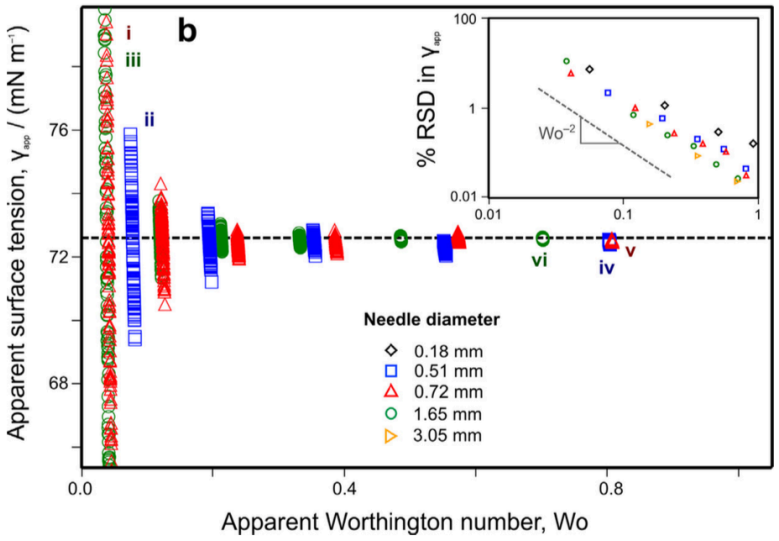

Figure 5.4 The inset shows the % relative standard deviation (%RSD) for each measurement set as a function of wo in ref. [28].

Two phenomena contribute to the reduction in interfacial tension of 5CB drop: (1) adsorption of EC nanoparticles at the water-5CB interface; and/or (2) alignment change of 5CB molecule at the interface. The latter is due to the fact that the IFT of a liquid

crystal-containing interface may be dependent on the alignment of the liquid crystal molecules at the interface, which and can be easily altered by the adsorption of any surface-active agents.

5.2 Analysis of Dynamic Interfacial Tension at Early Times

The early time dynamic IFT data can be analyzed in terms of equation (3). In this analysis, the early time IFT data is plotted against √t, as shown in Figure 5.5. The adsorption energy, $|\Delta E|$, is estimated from the slope of the linear regression. The estimated average adsorption energy is $(5.7 \pm 0.4)\times10^4 k_B T$ and $(6 \pm 1)\times10^4 k_B T$ for 0.3 g L^{-1} and 0.5 g L^{-1} EC nanoparticle solution, respectively. These two adsorption energy values calculated from two different EC nanoparticle bulk concentration are close to each other, which indicates that the adsorption energy of nanoparticles is independent of the bulk concentration, as expected. The intercept of the linear regression of early time IFT data provides an approach to estimate the IFT of 5CB in water without any nanoparticles. The interfacial tension γ_0 of 5CB in water has never been accurately measured due to the very small density difference between 5CB and water. Our estimations of interfacial tension γ_0 of 5CB in water are 38.5 ± 0.1 dyne cm^{-1} and 39.7 ± 0.3 dyne cm^{-1} from our two experiments with EC nanoparticle suspensions of different concentrations.

$$\gamma = \gamma_0 - 2N_A|\Delta E|C_0\sqrt{\frac{Dt}{\pi}} \tag{3}$$

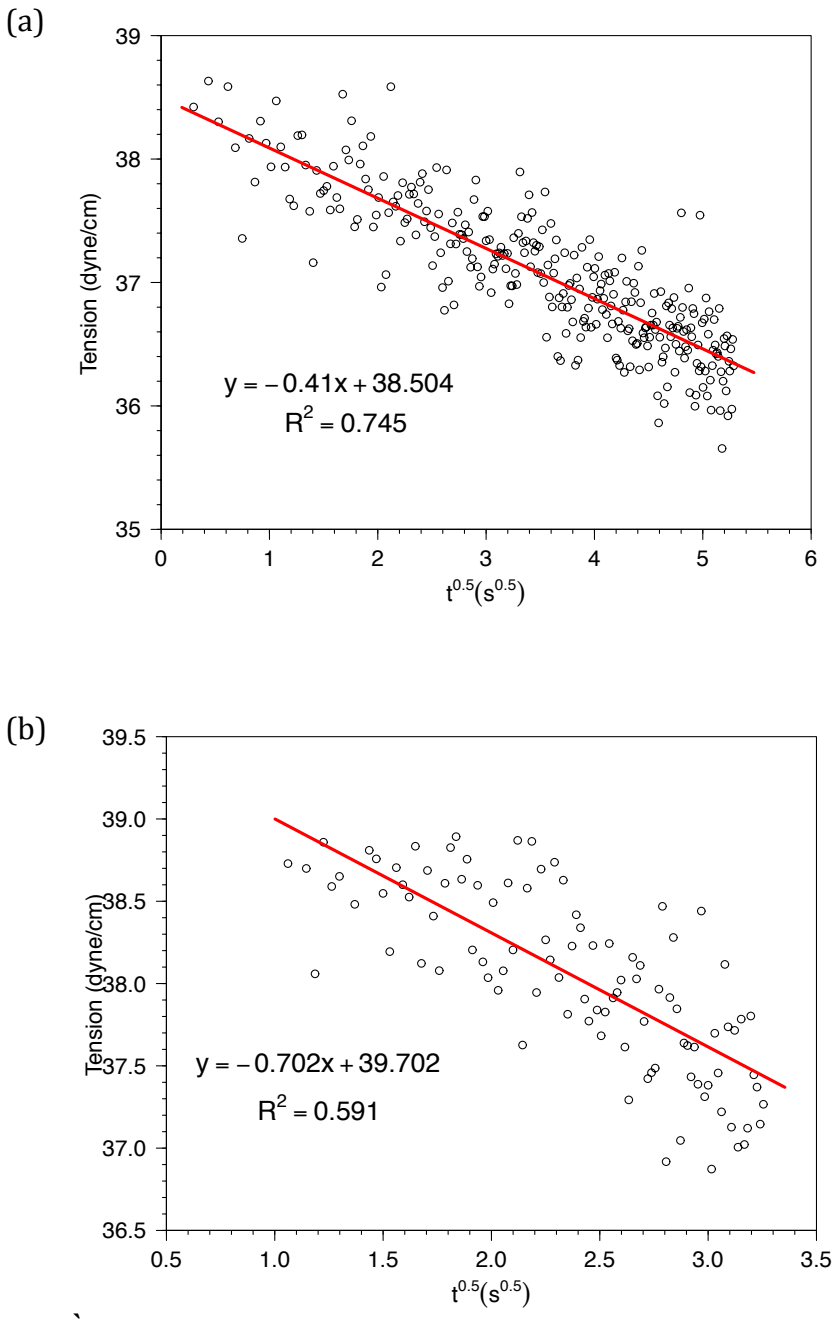

Figure 5.5 Exemplary plot of the early time dynamic IFT data of 5CB in EC nanoparticles with a bulk concentration of (a) 0.3 g L^{-1}; (b) 0.5 g L^{-1} Solid red lines show the linear regressions with parameters indicated in each panel.

5.3 Analysis of Dynamic Interfacial Tension at Late Times

The late time dynamic IFT data can be analyzed in terms of equation (4). Equation (4) demonstrates the linear relationship between late stages ($t \to \infty$) interfacial tension and $1/\sqrt{t}$. By plotting the late stages IFT data against $1/\sqrt{t}$, γ_∞ is obtained from the intercept of the linear regression as shown in Figure 5.6. For EC nanoparticle solution with a concentration of 0.3g L-1 and 0.5g L-1, the late time interfacial tension is 8.3 ± 0.04 dyne cm^{-1} and 9.4 ± 0.02 dyne cm^{-1}, respectively.

$$\gamma = \gamma_\infty + \frac{K_I |\Delta E|}{\left(\pi r^2\right)^2 N_A C_0} \sqrt{\frac{1}{Dt}} \tag{4}$$

(a)

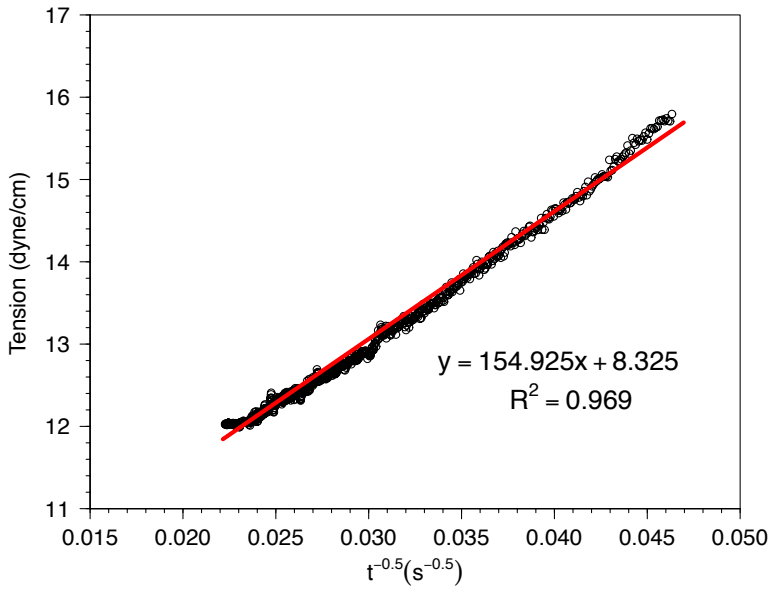

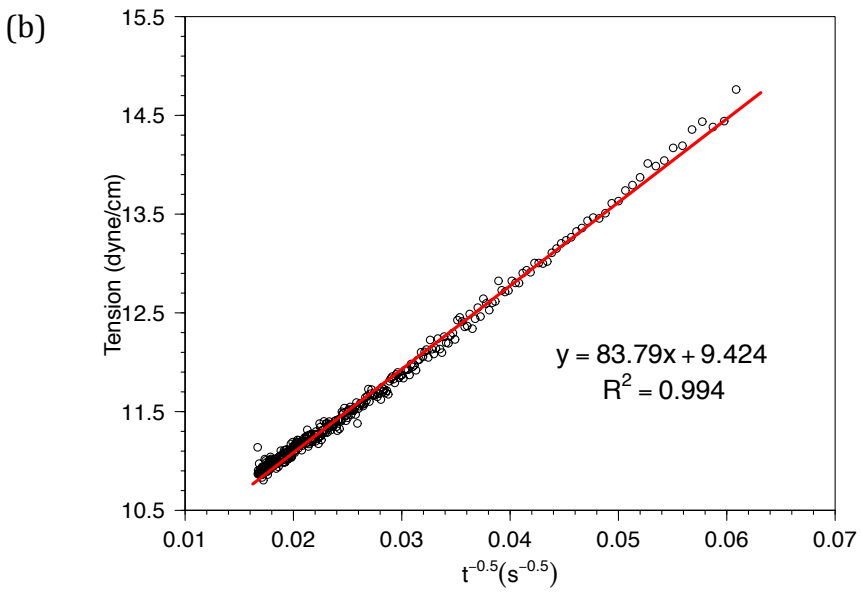

Figure 5.6 Exemplary plots of the late stages dynamic IFT data of 5CB in EC nanoparticles with a bulk concentration of (a) 0.3 g L^{-1} and (b) 0.5 g L^{-1}. Solid red lines show the linear regressions with parameters indicated in each panel.

5.4 Adsorption Energy ΔE using Pieranski's Approach

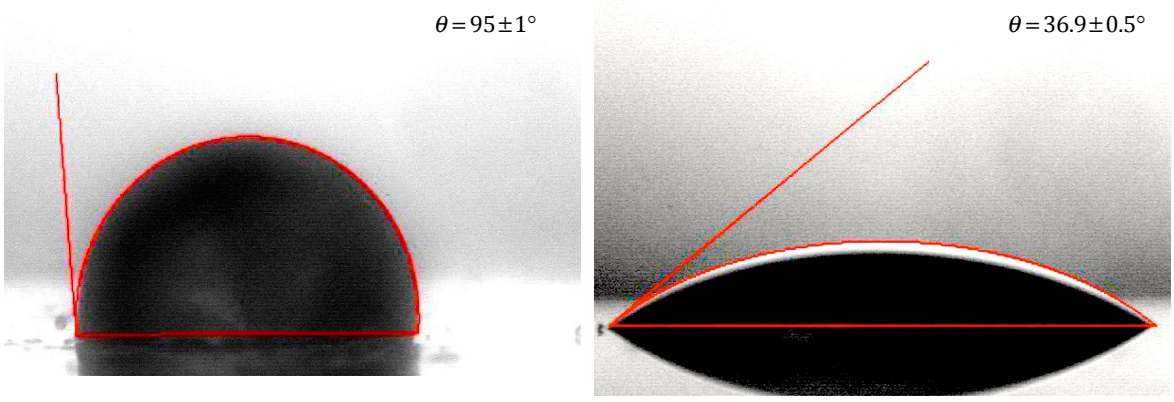

Figure 5.7 Contact angle images of 5CB in (1) water and (2) air. The glass substrates are coated with 4 wt.% EC in ethanol solution.

The Pieranski equation relates the reduction of the surface energy associated with the radius r of the adsorbed particle and its contact angle θ and is given by:

$$\left|\Delta E\right| = \gamma_0 \pi r^2 \left(1 - \left|\cos\theta\right|\right)^2 \quad (1)$$

Here, γ_0 is the interfacial tension of a pristine interface, which is directly obtained from the analysis of early time dynamic IFT data, and θ is the contact angle of a single particle at the interface measured through the aqueous phase. In order to calculate the adsorption energy $\left|\Delta E\right|$ from Pieranski's approach, it is necessary to measure the contact angle of 5CB angle in water. The contact angle of 5CB in air is also measured as shown in Figure 5.7. The contact angle of 5CB on EC against water is 95±1° and against air is 39.6± 0.5°. The images of contact angle are shown in Figure 5.7. The adsorption energy $\left|\Delta E\right|$ estimates from equation (3) compare very well to the calculations from equation (1), and are (5.0 ± 0.1)×$10^4$$k_B$T and (5.1 ± 0.1)×$10^4$$k_B$T for 0.3 g L^{-1} and 0.5 g L^{-1} nanoparticles solution, respectively.

5.5 Adsorption energy ΔE using Du et. al Approach

Du et. al proposed another approach to calculate the adsorption energy ΔE on the basis of thermodynamic considerations as below:

$$\left|\Delta E\right| = \frac{\gamma_0 - \gamma_\infty}{\Theta_\infty} \pi r^2 \quad (2)$$

Here, γ_0 and γ_∞ are obtained from early time and late time dynamic IFT data analysis. The surface coverage Θ_∞ of the interface at steady state, has been approximated by hexagonal close packing of nanoparticles ($\Theta_\infty = 0.91$) [25]. This approximation has been based on recent publications that demonstrate the hexagonal packing of nanoparticles formed at the water-LC interface. The adsorption energy based on Du's equation is calculated to be (5.0 ± 0.1)×$10^4$$k_B$T and (5.2 ± 0.1)×$10^4$$k_B$T for 0.3 g L^{-1} and 0.5 g L^{-1} nanoparticles solution, respectively. This approach to measure adsorption energy ΔE is an attractive alternative to Pieranski's equation, because measurement of interfacial

tension is much more straightforward than measurement of the contact angle θ of the adsorbed particle.

Nanoparticle concentration	Bizmark equation ΔE_1	Pieranski equation ΔE_2	Du et al. equation ΔE_3
0.3g L^{-1}	$(5.7 \pm 0.4)\times10^4 k_B T$	$(5.0 \pm 0.1)\times10^4 k_B T$	$(5.0 \pm 0.1)\times10^4 k_B T$
0.5g L^{-1}	$(6 \pm 1) \times10^4 k_B T$	$(5.1 \pm 0.1)\times10^4 k_B T$	$(5.2 \pm 0.1)\times10^4 k_B T$

Table 1. Comparisons of the adsorption energy ΔE calculated from three approaches.

The dynamic interfacial tension data of liquid crystal 5CB has been applied to Bizmark's equation to obtain the values of the pristine interfacial tension γ_0, the late time interfacial tension γ_∞ and the adsorption energy ΔE. Then γ_0 and γ_∞ are applied to the other two approaches to obtain the value of adsorption energy ΔE. The calculated results of the adsorption energy from three approaches compare very well to each other as shown in table 1, which proves that Bizmark's approach with the use of dynamic interfacial tension could be applied to study the adsorption process of nanoparticles onto anisotropic liquid crystal interfaces. These findings provide a quantitative method to study nanoparticle adsorption at liquid crystal interfaces.

5.6 A Novel Approach to Predict the Transient Interfacial Coverage of Nanoparticle

Elimination of $|\Delta E|$ between the equations of Pieranski and Du et al yields the following equation for the coverage of the interface:

$$\Theta_{\infty} = \frac{1-\frac{\gamma_{\infty}}{\gamma_0}}{\left(1-\left|\cos\theta\right|\right)^2} \tag{29}$$

In this equation, Θ_{∞} can be estimated from knowledge of the interfacial tensions γ_0 , γ_{∞} and contact angle θ. Equation 29 demonstrates a relationship of surface (interface) coverage Θ_{∞} with γ_{∞}, γ_0 and contact angle θ. As we discussed previously, the early stage interfacial tension γ_0 and the late time interfacial tension γ_{∞} could be obtained from the analysis of early stages and late stages IFT data respectively. With the dynamic interfacial tension data from our previous experiments, the greatest surface (interface) coverage Θ_{∞} is calculated to be 0.938 and 0.913 for 0.3g L^{-1} and 0.5 g L^{-1} EC nanoparticle solution, respectively. Our calculated results of surface (interface) coverage Θ_{∞} by nanoparticles compare well to the hexagonal close packing assumption ($\Theta_{\infty} = 0.91$) [25] from recent publications. Equation also provides a way to probe the transient surface (interface) coverage Θ_{∞} of nanoparticles onto water-LC interface. If we replace γ_{∞} in equation (29) with the transient interfacial tension γ at any time of dynamic adsorption process, the equation becomes:

$$\Theta = \frac{1-\frac{\gamma_{\infty}}{\gamma_0}}{\left(1-\left|\cos\theta\right|\right)^2} \tag{31}$$

Figure 5.8 illustrates the dynamic change process of surface (interface) coverage of EC nanoparticles at LC-water interface. EC nanoparticles in larger bulk concentration (0.5g L^{-1}) cover the LC-water interface faster than EC nanoparticles in 0.3 g L^{-1} EC solution. We are able to probe the transient surface (interface) coverage of nanoparticles at the water-LC interface with the knowledge of the transient interfacial tension at any moment. As a result, this approach has significant implications for the quantitative description of the transient surface (interface) coverage of nanoparticles adsorbed at the LC-water interface.

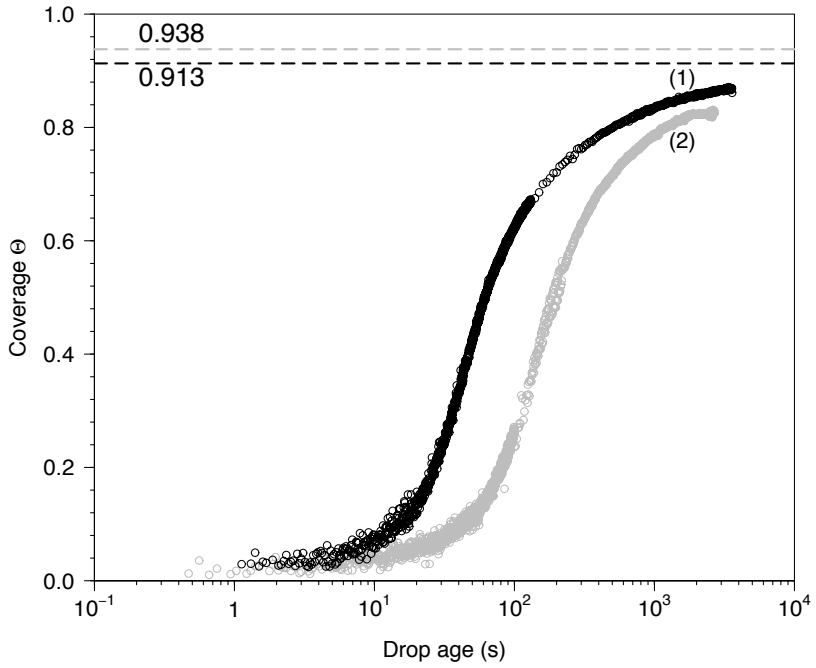

Figure 5.8 Plot of fractional surface coverage of EC nanoparticles in bulk EC concentration of (1) 0.5g L^{-1} and (2) 0.3g L^{-1} adsorbed at LC-water interface on a log scale of time. Dash lines are the calculated possible greatest surface coverage for each case.

5.7 Optical Study of Alignment of 5CB Molecules Induced by EC Nanoparticles

In order to investigate the effect of EC nanoparticles on the LC molecule alignment at the water-LC interface, we dropped a small amount of liquid crystal 5CB onto the water. We observed the spontaneous formation of a film of 5CB spreading over the water surface, with an easily interpreted optical appearance characteristic of planar anchoring at the water-LC interface under microscope with crossed polarizers (as shown in Figure 5.9), which is well-known as a "Schlieren" texture. The addition of EC nanoparticles to the water phase resulted in the dewetting of the 5CB film into a droplet. This phenomenon is exactly same observed by Brake et al. [14] upon the addition of surfactant SDS to the water phase.

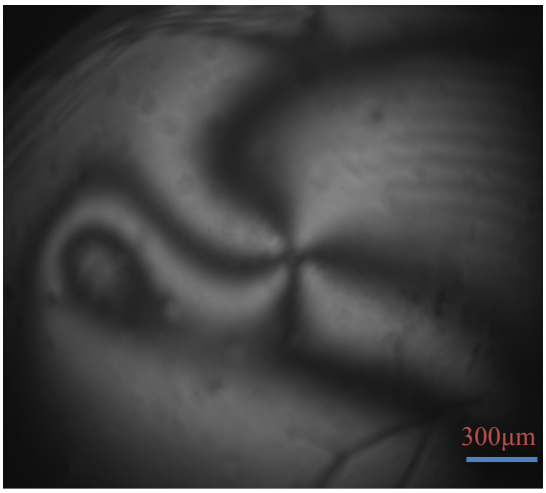

Figure 5.9 Optical images of 5CB deposited onto the surface of water. The image was obtained by orthoscopic examination between two crossed polarizers using a 10× magnifications.

Compared to a conventional interface between two isotropic phases, the interface containing an anisotropic liquid crystal often exhibits two unusual features [16,55]. First, in many cases, the interfacial tension of a nematic liquid crystal exhibits a maximum value at a temperature in the vicinity of the bulk nematic-isotropic transition temperature T_{NI} [55], while the interfacial tension of an isotropic phase always decreases with increasing temperature. For 5CB, the nematic-isotropic temperature is known to be 35.2 °C [54,56,57]. All our measurements were conducted under 22°C (295K), in which 5CB remains nematic. Second, the interfacial tension between a liquid crystal and isotropic phase may be strongly effected by the alignment of the LC molecule at the interface. In our previous discussion, we mentioned that adsorption of EC nanoparticles may induce an alignment change of 5CB molecules at the LC-water interface. The alignment change of 5CB molecules at the interface may contribute to the reduction of interfacial tension [45,46]. The optical test by polarized microscope aims to confirm if an alignment change of 5CB molecules at the interface induced by the adsorption of EC nanoparticles. The orientational ordering of 5CB molecules at LC-water interface is well known to be planar [58]. Optical tests under crossed polarizers of our optical cells show the obvious existence of birefringence (bright part of Figure 5.10) in the region where LCs are confined between two 4 wt% EC-treated glass substrates. This optical result is in a good agreement with previous optical test results of liquid crystal textures with a planar

alignment. This result shows that both the solvent water phase and EC nanoparticles contribute to inducing a planar alignment of 5CB molecules at the interface. As a conclusion, the adsorption of EC nanoparticles at the water-LC interface will not alter the alignment of 5CB molecules at the interface. This optical result further confirms that the reduction in interfacial tensions in the overall dynamic adsorption process can be attributed to the adsorption of EC nanoparticles at the interface, not to the alignment change of 5CB molecules at the water-LC interface.

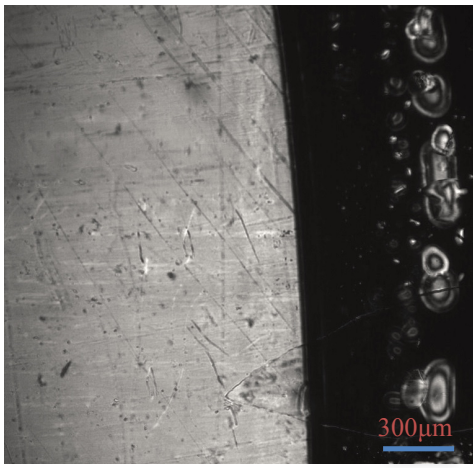

Figure 5.10 Optical images of 5CB confined between two glass substrates that were spin-coated 4 wt.% EC in ethanol solution to align the 5CB in a planar orientation. The thickness of the LC film was held constant at 19μm and observed at × 10 magnifications with crossed polarizers.

Chapter 6

Conclusions

Adsorption of ethyl cellulose (EC) nanoparticles at water and nematic liquid crystal 5CB interface results in significant reduction in interfacial tension of 5CB droplets. Adsorption of EC nanoparticles did not lead to transitions of 5CB molecules alignment at the interface. The irreversible adsorption model of colloidal particles developed by Bizmark et. al can be applied to study the dynamics of adsorption of colloidal nanoparticles onto anisotropic nematic interfaces. Analysis of dynamic interfacial tension data of liquid crystal 5CB provides a new method to measure the adsorption energy $|\Delta E|$ of EC nanoparticles, the early time interfacial tension γ_0 and the steady state interfacial tension γ_∞. The adsorption energy $|\Delta E|$ calculated in terms of Bizmark's approach compares well with results obtained from Pieranski's and Du's approach with the information of γ_0 and γ_∞ from previous analysis of dynamic interfacial tension data. The maximum surface coverage of nanoparticles at nematic 5CB liquid crystal interface at steady state further confirms the hexagonal close packing of nanoparticle assumed by other researchers. We also present a novel equation to probe the transient surface coverage of nanoparticles at the LC interface with the use of dynamic interfacial tension. These finding have significant implications for the quantitative description of nanoparticles adsorption at anisotropic nematic liquid crystal interfaces.

References

[1] V. J. Aliño, K. X. Tay, S. a. Khan, and K. L. Yang, "Inkjet printing and release of monodisperse liquid crystal droplets from solid surfaces," *Langmuir*, vol. 28, no. 41, pp. 14540–14546, 2012.

[2] I. Lin, D. S. Miller, P. J. Bertics, C. J. Murphy, J. J. De Pablo, and N. L. Abbott, "Crystalline Droplets," *Science (80-.).*, no. June, pp. 1297–1300, 2011.

[3] a. Fernández-Nieves, D. R. Link, and D. a. Weitz, "Polarization dependent Bragg diffraction and electro-optic switching of three-dimensional assemblies of nematic liquid crystal droplets," *Appl. Phys. Lett.*, vol. 88, no. 12, pp. 2004–2007, 2006.

[4] M. Humar, M. Ravnik, S. Pajk, and I. Muševič, "Electrically tunable liquid crystal optical microresonators," *Nat. Photonics*, vol. 3, no. 10, pp. 595–600, 2009.

[5] H. Yokoyama, "Liquid crystals: Tunable whispers," *Nat. Photonics*, vol. 3, no. 10, pp. 560–561, 2009.

[6] J. Yamamoto and H. Tanaka, "Transparent nematic phase in a liquid-crystal-based microemulsion.," *Nature*, vol. 409, no. 6818, pp. 321–325, 2001.

[7] O. D. Lavrentovich, "Topological defects in dispersed words and worlds around liquid crystals, or liquid crystal drops," *Liq. Cryst.*, vol. 24, no. 1, pp. 117–126, 1998.

[8] S. Sivakumar, K. L. Wark, J. K. Gupta, N. L. Abbott, and F. Caruso, "Liquid crystal emulsions as the basis of biological sensors for the optical detection of bacteria and viruses," *Adv. Funct. Mater.*, vol. 19, no. 14, pp. 2260–2265, 2009.

[9] M. I. Kinsinger, M. E. Buck, N. L. Abbott, and D. M. Lynn, "Immobilization of polymer-decorated liquid crystal droplets on chemically tailored surfaces," *Langmuir*, vol. 26, no. 12, pp. 10234–10242, 2010.

[10] O. Tongcher, R. Sigel, and K. Landfester, "Liquid crystal nanoparticles prepared as miniemulsions," *Langmuir*, vol. 22, no. 10, pp. 4504–4511, 2006.

[11] V. J. Aliño, J. Pang, and K. L. Yang, "Liquid crystal droplets as a hosting and sensing platform for developing immunoassays," *Langmuir*, vol. 27, no. 19, pp. 11784–11789, 2011.

[12] K. a. Simon, P. Sejwal, R. B. Gerecht, and Y. Y. Luk, "Water-in-water emulsions stabilized by non-amphiphilic interactions: Polymer-dispersed lyotropic liquid crystals," *Langmuir*, vol. 23, no. 3, pp. 1453–1458, 2007.

[13] N. L. Abbott, S. Sivakumar, J. K. Gupta, and F. Caruso, "Monodisperse emulsions through templating polyelectrolyte multilayer capsules," *Chem. Mater.*, vol. 20, no. 6, pp. 2063–2065, 2008.

[14] J. M. Brake and N. L. Abbott, "An experimental system for imaging the reversible adsorption of amphiphiles at aqueous-liquid crystal interfaces," *Langmuir*, vol. 18, no. 16, pp. 6101–6109, 2002.

[15] N. a. Lockwood and N. L. Abbott, "Self-assembly of surfactants and phospholipids at interfaces between aqueous phases and thermotropic liquid crystals," *Curr. Opin. Colloid Interface Sci.*, vol. 10, no. 3–4, pp. 111–120, 2005.

[16] J. W. Kim, H. Kim, Lee Myoungbae, and J. J. Magda, "Interfacial tension of a nematic liquid crystal/water interface with homeotropic surface alignment," *Langmuir*, vol. 20, no. 19, pp. 8110–8113, 2004.

[17] J. M. Brake, A. D. Mezera, and N. L. Abbott, "Effect of Surfactant Structure on the Orientation of Liquid Crystals at Aqueous - Liquid Crystal Interfaces †," no. C, pp. 6436–6442, 2003.

[18] J. a. Moreno-Razo, E. J. Sambriski, N. L. Abbott, J. P. Hernández-Ortiz, and J. J. de Pablo, "Liquid-crystal-mediated self-assembly at nanodroplet interfaces," *Nature*, vol. 485, no. 7396, pp. 86–89, 2012.

[19] B. P. Binks, "Particles as surfactants—similarities and differences," *Curr. Opin. Colloid Interface Sci.*, vol. 7, no. 1–2, pp. 21–41, 2002.

[20] B. P. Binks and R. Murakami, "Phase inversion of particle-stabilized materials from foams to dry water.," *Nat. Mater.*, vol. 5, no. 11, pp. 865–869, 2006.

[21] S. Crossley, J. Faria, M. Shen, and D. E. Resasco, "Solid nanoparticles that catalyze biofuel upgrade reactions at the water/oil interface.," *Science*, vol. 327, no. 5961, pp. 68–72, 2010.

[22] M. Rahimi, T. F. Roberts, J. C. Armas-Pérez, X. Wang, E. Bukusoglu, N. L. Abbott, and J. J. de Pablo, "Nanoparticle self-assembly at the interface of liquid crystal droplets," *Proc. Natl. Acad. Sci.*, vol. 112, no. 17, p. 201422785, 2015.

[23] X. Wang, D. S. Miller, J. J. de Pablo, N. L. Abbott, J. De Pablo, and N. L. Abbott, "Organized assemblies of colloids formed at the poles of micrometer-sized droplets of liquid crystal.," *Soft Matter*, vol. 10, no. 44, pp. 8821–8, 2014.

[24] L. Hu, M. Chen, X. Fang, and L. Wu, “Oil–water interfacial self-assembly: a novel strategy for nanofilm and nanodevice fabrication,” *Chem. Soc. Rev.*, vol. 41, no. 3, p. 1350, 2012.

[25] K. Du, E. Glogowski, T. Emrick, T. P. Russell, and A. D. Dinsmore, “Adsorption energy of nano- and microparticles at liquid-liquid interfaces,” *Langmuir*, vol. 26, no. 15, pp. 12518–12522, 2010.

[26] N. Bizmark, M. a. Ioannidis, and D. E. Henneke, “Irreversible adsorption-driven assembly of nanoparticles at fluid interfaces revealed by a dynamic surface tension probe,” *Langmuir*, vol. 30, no. 3, pp. 710–717, 2014.

[27] R. B. Bird, W. E. Stewart, and E. N. Lightfoot, *Transport Phenomena*. 1960.

[28] J. D. Berry, M. J. Neeson, R. R. Dagastine, D. Y. C. Chan, and R. F. Tabor, “Measurement of surface and interfacial tension using pendant drop tensiometry,” *J. Colloid Interface Sci.*, vol. 454, pp. 226–237, 2015.

[29] I. Dierking, *Textures of liquid crystals*. 2003.

[30] Http://physics.berkeley.edu/research/yildiz/Teaching/PHYS250/Lecture_PDFs/polarization%20microscopy.pdf, “Basics of Polarizing Microscopy,” *Olympus*, p. 28.

[31] M. Boussoualem and F. Roussel, “Soft Matter dielectric and electro-optical properties of nematic droplets dispersed in a polymer network,” pp. 367–373, 2014.

[32] V. B. Fainerman, a. V. Makievski, and R. Miller, “The analysis of dynamic surface tension of sodium alkyl sulphate solutions, based on asymptotic equations of adsorption kinetic theory,” *Colloids Surfaces A Physicochem. Eng. Asp.*, vol. 87, no. 1, pp. 61–75, 1994.

[33] N. a. Lockwood, K. D. Cadwell, F. Caruso, and N. L. Abbott, “Formation of polyelectrolyte multilayer films at interfaces between thermotropic liquid crystals and aqueous phases,” *Adv. Mater.*, vol. 18, no. 7, pp. 850–854, 2006.

[34] E. Tjipto, K. D. Cadwell, J. F. Quinn, A. P. R. Johnston, N. L. Abbott, and F. Caruso, “Tailoring the interfaces between nematic liquid crystal emulsions and aqueous phases via layer-by-layer assembly,” *Nano Lett.*, vol. 6, no. 10, pp. 2243–2248, 2006.

[35] G. Foffano, J. S. Lintuvuori, a. Tiribocchi, and D. Marenduzzo, “The dynamics of colloidal intrusions in liquid crystals: a simulation perspective,” *Liq. Cryst. Rev.*, no. April, pp. 1–27, 2014.

[36] T. Araki and H. Tanaka, “Colloidal aggregation in a nematic liquid crystal: Topological arrest of particles by a single-stroke disclination line,” *Phys. Rev. Lett.*, vol. 97, no. 12, pp. 1–4, 2006.

[37] N. Hijnen, T. a. Wood, D. Wilson, and P. S. Clegg, “Self-organization of particles with planar surface anchoring in a cholesteric liquid crystal,” *Langmuir*, vol. 26, no. 16, pp. 13502–13510, 2010.

[38] a Nych, U. Ognysta, M. Skarabot, M. Ravnik, S. Zumer, and I. Muševič, “Assembly and control of 3D nematic dipolar colloidal crystals.,” *Nat. Commun.*, vol. 4, p. 1489, 2013.

[39] J. C. Loudet, P. Barois, P. Auroy, P. Keller, H. Richard, and P. Poulin, “Colloidal structures from bulk demixing in liquid crystals,” *Langmuir*, vol. 20, no. 26, pp. 11336–11347, 2004.

[40] M. Ravnik, M. Škarabot, S. Žumer, U. Tkalec, I. Poberaj, D. Babič, N. Osterman, and I. Muševič, “Entangled nematic colloidal dimers and wires,” *Phys. Rev. Lett.*, vol. 99, no. 24, pp. 1–4, 2007.

[41] L. Isa, E. Amstad, K. Schwenke, E. Del Gado, P. Ilg, M. Kröger, and E. Reimhult, “Adsorption of core-shell nanoparticles at liquid–liquid interfaces,” *Soft Matter*, vol. 7, no. 17, p. 7663, 2011.

[42] J. Eastoe and J. S. Dalton, “Dynamic surface tension and adsorption mechanisms of surfactants at the air-water interface,” *Adv. Colloid Interface Sci.*, vol. 85, no. 2, pp. 103–144, 2000.

[43] R. Hogg, T. W. Healy, and D. W. Fuerstenau, “Mutual coagulation of colloidal dispersions,” *Trans. Faraday Soc.*, vol. 62, no. 615, p. 1638, 1966.

[44] Z. Adamczyk, “Kinetics of Diffusion-Controlled Adsorption of Colloid Particles and Proteins.,” *J. Colloid Interface Sci.*, vol. 229, no. 2, pp. 477–489, 2000.

[45] S. Krishnaswamy and R. Shashidhar, “Experimental Studies of the Surface Tension of Nematic Liquid Crystals,” *Mol. Cryst. Liq. Cryst.*, vol. 35, no. 3–4, pp. 253–259, 1976.

[46] L. M. Tarakhan and L. M. Tarakhan, “Determination of the surface tension of 5CB liquid crystal by the pendant drop method.,” *Ukr. J. Phys.*, vol. 51, pp. 22–26, 2006.

[47] M. Tintaru, R. Moldovan, T. Beica, and S. Frunza, “Surface tension of some liquid crystals in the cyanobiphenyl series,” *Liq. Cryst.*, vol. 28, no. 5, pp. 793–797, 2001.

[48] M. G. J. Gannon and T. E. Faber, “The surface tension of nematic liquid crystals,” *Philos. Mag. A*, vol. 37, no. 1, pp. 117–135, 1978.

[49] S. Zeppieri, J. Rodríguez, and a. L. López De Ramos, “Interfacial tension of alkane + water systems,” *J. Chem. Eng. Data*, vol. 46, no. 5, pp. 1086–1088, 2001.

[50] D. a. Dunmur and W. H. Miller, “Volumetric Studies of the Homologous Series of Alkyl-Cyano-Biphenyl Liquid Crystals,” *Le J. Phys. Colloq.*, vol. 40, no. C3, pp. C3–141–C3–146, 1979.

[51] H. Jin, W. Zhou, J. Cao, S. D. Stoyanov, T. B. J. Blijdenstein, P. W. N. de Groot, L. N. Arnaudov, and E. G. Pelan, “Super stable foams stabilized by colloidal ethyl cellulose particles,” *Soft Matter*, vol. 8, no. 7, p. 2194, 2012.

[52] S. Ferdous, M. a. Ioannidis, and D. Henneke, “Adsorption kinetics of alkanethiol-capped gold nanoparticles at the hexane-water interface,” *J. Nanoparticle Res.*, vol. 13, no. 12, pp. 6579–6589, 2011.

[53] J. Deschamps, J. P. M. Trusler, and G. Jackson, “Vapor pressure and density of thermotropic liquid crystals: MBBA, 5CB, and novel fluorinated mesogens,” *J. Phys. Chem. B*, vol. 112, no. 13, pp. 3918–3926, 2008.

[54] C. Carboni, S. Al-Ruzaiqi, a. Al-Siyabi, S. Al-Harthi, a. K. George, and T. J. Sluckin, “The behaviour of the interfacial surface tension of liquid-crystal materials in the vicinity of the nematic-isotropic phase transition,” no. July 2015, 2008.

[55] T. Beica, R. Moldovan, I. Zgura, and S. Frunza, “Interfacial tension of some liquid crystals in the cyanobiphenyl series at the interface with glycerol,” *J. Optoelectron. Adv. Mater.*, vol. 9, no. 11, pp. 3624–3627, 2007.

[56] G.-H. Chen and J. Springer, “Surface Phenomena of Liquid Crystalline Substances,” *Mol. Cryst. Liq. Cryst. Sci. Technol. Sect. A. Mol. Cryst. Liq. Cryst.*, vol. 326, no. 1, pp. 1–14, 1999.

[57] M. M. Telo da Gama, “The interfacial properties of a model of a nematic liquid crystal,” *Mol. Phys.*, vol. 52, no. 3, pp. 611–630, 1984.

[58] J. Zou and J. Fang, “Director configuration of liquid-crystal droplets encapsulated by polyelectrolytes,” *Langmuir*, vol. 26, no. 10, pp. 7025–7028, 2010.

[59] Wikipedia, 'Liquid crystal', 2015. [Online]. Available: https://en.wikipedia.org/wiki/Liquid_crystal. [Accessed: 15- Sep- 2015].

[60] Aztec.ms.northwestern.edu, 'WILLIAM KUNG on the Web - Polar Liquid Crystals', 2015. [Online]. Available: http://aztec.ms.northwestern.edu/wkung/lc.html. [Accessed: 15- Sep- 2015].

[61] Bly.colorado.edu, 'Liquid Crystal Textures', 2015. [Online]. Available: https://bly.colorado.edu/lcphysics/textures/. [Accessed: 15- Sep- 2015].

[62] Wikipedia, 'Ethyl cellulose', 2015. [Online]. Available: https://en.wikipedia.org/wiki/Ethyl_cellulose. [Accessed: 15- Sep- 2015].

[63] Yang, C. Dicko, C. Bain, Z. Gong, R. Jacobs, Z. Shao, A. Terry and F. Vollrath, 'Behavior of silk protein at the airâ€“water interface', *Soft Matter*, vol. 8, no. 37, p. 9705, 2012.

[64] Face-kyowa.co.jp, 'What is Surface Tension? :Kyowa Interface Science', 2015. [Online]. Available: http://www.face-kyowa.co.jp/english/en_science/en_theory/en_what_Surface_tension/. [Accessed: 15- Sep- 2015].

[65] Solarnenergy.com, 'SNE Research', 2015. [Online]. Available: http://www.solarnenergy.com/kor/pr_service/analyst_show.php?sub_cat=3&bbsId=4953&tbl=column. [Accessed: 15- Sep- 2015].

[66] Plc.cwru.edu, 'Introduction to Liquid Crystals', 2015. [Online]. Available: http://plc.cwru.edu/tutorial/enhanced/files/lc/intro.htm. [Accessed: 21- Sep- 2015].

[67] B. Senyuk, 'Liquid Crystals: a Simple View on a Complex Matter', *Personal.kent.edu*, 2015. [Online]. Available: http://www.personal.kent.edu/~bisenyuk/liquidcrystals/. [Accessed: 21- Sep- 2015].

[68] J. M. Lu, H. D. Zhang, J. D. Ding, and Y. L. Yang, “Director configurations of nematic liquid crystalline droplets and corresponding configuration transitions,” *Science in China Series B-Chemistry*, vol. 39, no. 2. pp. 203–210, 1996.

[69] M. Kanke and K. Sasaki, “Equilibrium configuration in a nematic liquid crystal droplet with homeotropic anchoring of finite strength,” *J. Phys. Soc. Japan*, vol. 82, no. 9, 2013.